Catalysis Science & Technology

Accepted Manuscript

This article can be cited before page numbers have been issued, to do this please use: A. Dewaele, B. Van Berlo, J. Dijkmans, P. A. Jacobs and B. F. Sels, *Catal. Sci. Technol.*, 2015, DOI: 10.1039/C5CY01897H.

ROYAL SOCIETY OF CHEMISTRY

www.rsc.org/catalysis

View Article Online
DOI: 10.1039/C5CY01897H

Catalysis Science and Technology

ARTICLE

Immobilized Grubbs Catalysts on Mesoporous Silica Materials: Insight into Support Characteristics and Their Impact on Catalytic Activity and Product Selectivity

Received 00th January 20xx,
Accepted 00th January 20xx

DOI: 10.1039/x0xx00000x

www.rsc.org/

A. Dewaele[a], B. Van Berlo[a], J. Dijkmans[a], P. Jacobs[a], B. Sels[a]

Silica materials show a high ability to physisorb the 2nd generation Hoveyda-Grubbs catalyst (HG2) in organic solvents. The interaction with the complex, likely proceeding through hydrogen bonding, is particularly strong with surfaces rich in silanols, geminal silanols showing the highest affinity, and therefore mesoporous silica are the supports of choice. As long as the silica material is sufficiently pure and free of cages, in which high HG2 concentrations can accumulate, the immobilisation of HG2 occurs very stable. Despite the complex stability, exploration of HG2 loaded mesoporous silica supports in metathesis of *cis*-cyclooctene indicated significant diffusional and confinement effects, and therefore control of pore size, pore architecture and morphology in balance with the intrinsic catalytic activity, is essential in the catalyst design. As metathesis of *cis*-cyclooctene apparently proceeds through initial formation of linear polymers, followed by backbiting forming the cyclic oligomers, potential interference of mass transport and space restriction issues is not surprising. This study shows that the catalyst requirements are best met with the TUD-1 silica support (1.24 wt% HG2). Under such conditions, the heterogeneous catalyst performes as good as the homogeneous one, presenting the thermodynamic distribution of cyclic oligomers. The latter catalyst also showed a high catalyst stability in a continuous fixed bed reactor, corresponding to 18000 catalytic turnover numbers. Catalytic rates and catalyst stability are lower when operating in diffusional regime, therefore long reaction times are required to reach the thermodynamic product distribution. Water removal from the catalyst is also important, not because of HG2 stability reasons, but lower reactions rates were measured for hydrated samples, likely due to inhibition of *cis*-cyclooctene uptake in the pores. Mild removal of physisorbed water before immobilization is therefore advised, for instance by thermal treatments, but care has to be taken to keep the silanol density high for firm HG2 immobilization and also to avoid formation of reactive siloxanes, which chemically react with and destroy HG2. Surprisingly, reactive siloxane formation conditions strongly depend on the silica type, TUD-1 being fairly sensitive to their formation. Finally, the best HG2 loaded TUD-1 catalyst is used successfully in a broad set of other metathesis reactions.

Introduction

Olefin metathesis exchanges alkyl substituents between olefins and is considered as a very important reaction for a wide range of applications in organic chemistry.[1-3] The reaction also provides nice opportunities to produce unsaturated and therefore modifiable polymers.[4] Well-defined commercially available Grubbs complexes are established as one of the most promising catalysts; they exhibit a high catalytic activity at ambient conditions and they show great tolerance towards functional groups, air and moisture.[5, 6] Despite of the industrial demonstrations,[7] their use has not been fully exploited due to high cost and environmental reasons. The latter issue is typically symbolized by a difficult catalyst recovery, leading to Ru-contamination of the product. This is disastrous in the production of fine chemicals like pharmaceuticals,[8-10] but it also implies a loss of precious metal.

Catalyst immobilization on a solid support offers an attractive solution to Ru recovery. The catalyst is not only more practical to separate from the product mixture, immobilization also allows protection against catalyst deactivation, caused by reported bimolecular decomposition pathways,[11-13] and even may exert beneficial confinement effects on conversion rate and product selectivity. The first heterogeneous metathesis catalysts were based on metal oxides or organometallic complexes on silica/alumina. Pioneer work of the surface organometallic chemistry was delivered by Basset and Copéret, *et al.*[14, 15], who characterized the active sites with NMR spectroscopy.[16-18] Several classical strategies have been developed to anchor Grubbs-like complexes to the surface through covalent linkage via: (a) halide ligands,[19-25] (b) phosphine ligands or N-heterocyclic carbenes (NHC) [11, 26-36] and (c) alkylidene ligands,[37-50] or through encapsulation in cage-like pore structures followed by post-reducing the window size

[a] Center for Surface Chemistry and Catalysis, KU Leuven, Celestijnenlaan 200F, 3001 Leuven, Belgium.

† Electronic Supplementary Information (ESI) available: Stirring experiments of HG2/MCM-41, correlation plots of ordered mesoporous silica, conversion plots of thermally treated TUD-1 and MCM-41 are provided. (Near)-infrared spectra and nitrogen physisorption measurements of thermally treated TUD-1 and MCM-41, information about ring-chain equilibria and additional ring selectivity experiments are given, See DOI: 10.1039/x0xx00000x

through silylation.[51, 52] Recent publications with regard to these strategies are summarized in excellent reviews.[53-57] Whereas these immobilization approaches often require a sophisticated and laborious synthesis, with alterations of both support and catalytic complex, an elegant and more practical immobilization strategy of Hoveyda-Grubbs (HG) complexes on silica supports was reported by Van Berlo *et al*.[58] This novel immobilization strategy is based on a subtle physical interaction between the 2nd generation Hoveyda-Grubbs (HG2) and the silica surface. Its synthesis avoids complicated modifications of either catalyst partner, therefore being industrially very attractive. Though the soft adsorption concept has been studied briefly and its application expanded successfully by others to new ordered mesoporous silica (OMS) like MCM-41 and SBA-15, there is no real consensus on the requirements of the support material of choice.[59-65]

Next to the high activity of the physically sorbed complexes, shifts in product selectivity between polymerization (ROMP) and ring-opening ring-closing metathesis (RO-RCM) were reported, especially in metathesis of cyclooctene.[59, 60, 66] The products of RO-RCM of cyclooctene, *viz*. macrocyclic structures, exhibit unique properties compared to their linear counterparts due to the lack of chain ends,[67, 68] making them potential intermediates as lubricants or plasticizers,[69, 70] but also in the fragrance industries.[71]

Despite the recent evaluation of different porous silica materials, no fundamental was delivered since, to unambiguously clarify the textural and structural requirements of the mesoporous silica to perform fast and stable metathesis. In search for the ideal catalyst support for RO-RCM of *cis*-cyclooctene to macrocycles, we undertook a systematic study to understand better the impact of the support properties (e.g. pore size, pore morphology) on the catalytic activity and product selectivity of supported HG2, as well as to assess surface properties that could substantially affect surface adsorption affinity and catalyst stability such as catalyst surface loading, silanol density and type. Furthermore, we addressed typical heterogeneous catalysis aspects like stability in a continuous reaction and discussed mass transfer limitations, rather uncommon in metathesis studies, but necessary to understand heterogeneous metathesis catalysis. Based on the insight, an optimal support-catalyst system is designed and further used to unravel the reaction pathways of RO-RCM of *cis*-cyclooctene to cyclic oligomers under heterogeneous catalysis conditions. The kinetic study clearly shows kinetic dissimilarities between homo- and heterogeneous reactions due to pore-related issues, all of this being dependent on the type of support and on the active site density. Finally, other metathesis types, for which no oligomers and polymers are formed, are also illustrated with the best supported HG2 catalyst.

Results and discussion

Screening of micro- and mesoporous silica

Various potential silica supports such as silica gels, zeolites and OMS were explored to support HG2. The immobilized catalysts were compared for their activity in metathesis of *cis*-cyclooctene, as this substrate is generally used to study the catalytic activity of porous catalysts.[26, 59, 60, 62, 64, 72] Moreover, it is an interesting probe to investigate the impact of textural properties on selectivity, as both cyclic and linear oligomers/polymers are formed. Table 1 compares the catalytic performance along with the material's characteristics. The activity is defined by the initial turnover frequency (TOF_i), i.e. the number of moles of cyclooctene converted per mol Ru per second, in the initial phase of the reaction.

Three zeolites were tested: Silicalite-1, $AlPO_4$-5 and Si-VPI-5 (Table 1, entry 2-4). The pores of Silicalite-1 and $AlPO_4$-5 are obviously too small for adsorption of HG2 (1.18 x 1.07 nm) and therefore contain very little Ru. Si-VPI-5 has larger pores (1.1 nm) and does adsorb HG2, but the density of hydroxyl groups on its surface, affording anchor points for the complex,[58] is very low resulting in low Ru loading. None of the zeolites showed a true heterogeneous activity. The few complexes present on the material leached into the solution, as was proven by a split-test. In such test, after 15 minutes reaction, part of the reaction suspension was removed and separated by filtration and transferred into a new vial. The reaction progress of the filtered sample was compared to that of the remaining reaction mixture at different time intervals. The result of HG2/Si-VPI-5, given in Figure 1A, shows a catalytic contribution owing to soluble HG2.

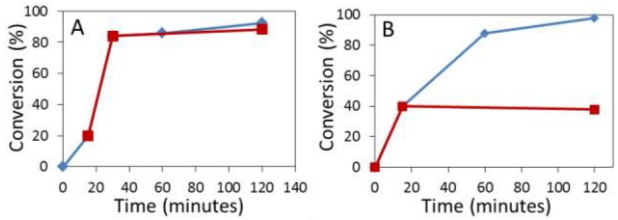

Figure 1. Two examples of a split-test with Ru leaching for A) HG2/Si-VPI-5 and without Ru leaching for B) HG2/TUD-1. Blue curve: Liquid phase with the heterogeneous catalyst; Red curve: liquid phase after filtration. Reaction conditions: 0.05 M *cis*-cyclooctene; 5 mL hexane; 50 mg HG2/Si-VPI-5 (pre-treated at 50 °C, 0.12 wt% Ru) or HG2/TUD-1 (pre-treated at 150 °C; 0.21 wt% Ru); 35 °C.

In contrast, the porous amorphous silica materials like silica gels and OMS are truly heterogeneous, confirming the essential role of surface silanols to firmly anchor HG2. The split-test of HG2/TUD-1 is illustrated in Figure 1B. Clearly, no activity is measured in the filtrate. Besides showing stable heterogeneous catalysis, the silica gels (Table 1, entry 5-6) are reasonable active, with TOF_i's ranging between 4 to 4.5 $s^{-1}.10^{-2}$. The lower values, compared to some OMS, may be due to the presence of impurities like Na (up to 0.06 %) and Ca (0.1 %), which modify the surface properties, leading to deactivation of HG2, as suggested in literature.[73]

The current wealth of existing OMS should allow a deeper analysis of the relationship between structural and surface characteristics and the catalytic performance (Table 1, entry 7-17). However, our experience reveals a blurred analysis due to a multi-variance of parameters and therefore drawing general conclusions on activity dependence of *e.g.*, particle size ($d_{particle}$) (Figure S1) and pore size (Figure S2), based on the

whole data set, is not always straightforward. To verify therefore the effect of pore size, three hexagonally pore-ordered mesoporous silicates (MCM-41) having pore diameters of respectively 2.6, 3.3 and 3.6 nm,[74] were tested (Table 1, entry 14-16). Comparable TOF_i's, 7.5 to 8.5 $s^{-1}.10^{-2}$ were shown, whereas SBA-3 (Table 1, entry 10), a mesoporous silica with similar pore architecture as MCM-41 and similar pore volumes and BET surface area, but a smaller pore diameter of 1.8 nm, showed a lower activity (TOF_i = 3 $s^{-1}.10^{-2}$). Mass transfer issues, depending on HG2 loading, seem to play a role in cyclooctene metathesis and impact the observed rate and selectivity. Though this point will be addressed later, it is fair to conclude at this stage that 2.5 nm pores (or larger) are recommended to efficiently catalyze *cis*-cyclooctene metathesis in presence of 0.2-0.4 wt% Ru loaded catalysts.

Besides pore diameter, morphology also plays a key role. To prove this, SBA-15 was synthesized in two different morphologies with comparable particle and pore size, and loaded with equal contents of HG2: rope-like (Table 1, entry 13) and fiber-like (Table 1, entry 9). Rope-like structures are typical for SBA-15 and have straight channels, whereas fibre-like structures have curving or orbicular channel structures. Though being instrumental to hold the catalyst in the pores, corrugated pores are unfavourable for molecular pore diffusion.[75] As rope-like SBA-15 performs 2.5 times better than the fibre-like SBA-15, intraparticle diffusion is a critical parameter. Additionally, as a large part of the pore volume of rope-like SBA-15 is occupied by micropores (inside the pore walls), not every catalytic complex might be accessible, which then could lead to a lower TOF_i.

Notably, HG2/KIT-5 and HG2/SBA-16 (Table 1, entry 7 and 8) gave the lowest activity of the OMS (TOF_i of 1.5 and 2 $s^{-1}.10^{-2}$ respectively), despite their high surface area and large pore size. These two silicas have 3D pore structures with a pronounced cage-like pore system. As the large cages of 5-8 nm allows formation of large oligomers/polymers of *cis*-cyclooctene, rate retardation is likely a result of internal pore entrance blockage. In addition, we also noticed that HG2 deactivates rapidly within the cage-like KIT-5 and SBA-16 silica, as visually seen by the fast green-to-brown colour change. As the colour variation occurred also in absence of substrate, deactivation is likely caused by fast disproportionation of HG2 due to a high concentration of HG2 and dynamics in the large cages.[76] Assuming HG2 is preferentially located inside the cages and its volume covers a minor part of the total volume (11 %)[77], the volumetric concentration in the pores of KIT-5 can be 35 times higher compared to fibre-like SBA-15 (1000 mol Ru m^{-3} *vs.* 29 mol Ru m^{-3}). HG2 is more evenly spread in fibre-like SBA-15, indicating that the low activity of this catalyst is likely caused by low diffusion through the corrugated pore system.

KIT-6 and MCM-48 (Table 1, entry 11 and 12), cubic Ia3d structures with a 3D channel network, have similar TOF_i's of 5 and 5.5 $s^{-1}.10^{-2}$ respectively, which is lower than one-dimensional hexagonal structures like MCM-41 and SBA-15. Despite their 3D pore network, pore diffusion might be slower due to a higher tortuosity (τ). For instance, linear hexagonal structures like MCM-41 and SBA-15 (Table 1, entry 13) have a τ close to 1, whereas τ = 3 for MCM-48.[78]

TUD-1, a highly porous structure with interconnecting cage-free mesopores, attains a high activity close to SBA-15 and MCM-41 (Table 1, Entry 17). Just like KIT-6 and MCM-48, it has a three-dimensional pore network, albeit a higher activity is observed. This could likely be attributed to the high porosity and pore structure of TUD-1, providing optimal features for fast intracrystalline diffusion. Awaiting for a profound structural analysis of TUD-1, other factors cannot be excluded. Nevertheless, TUD-1 has often been acknowledged in literature for its superior catalytic activity, outperforming other ordered mesoporous silica.[79-81]

To conclude, metathesis of *cis*-cyclooctene with low loadings of HG2 on mesoporous silica is truly heterogeneous, but care has to be taken to balance diffusion and the internal catalytic activity in order to perform catalysis in the kinetic regime and thus to use the costly HG2 most efficiently. Pure siliceous mesoporous silica are recommended, preferably with pores larger than 2.5 nm, absence of cage-like or bimodal pore systems, and a short diffusion path, which are morphology and pore architecture related. Rope-like SBA-15, spherical MCM-41 and TUD-1 are the support candidates of choice for *cis*-cyclooctene metathesis, because of absence of diffusion limitations. Their catalytic activity approaches that of the homogeneous complex (Table 1, entry 1).

Influence of solvent polarity on surface mobility and HG2 leaching

For all porous amorphous silica, irrespective of the particle size, pore size and pore ordering, HG2 remains grafted on the silica surface, as demonstrated above in the catalyst split-tests. To further confirm the true heterogeneity of the catalyst, an additional test was developed to examine the mobility of the complex under reaction conditions. The experiment is illustrated and described in Figure 2 for silica gel, but the conclusion holds for the other mesoporous silicas.

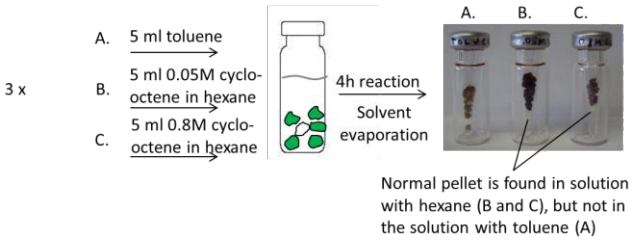

Figure 2. Mobility experiment to prove firm anchoring of HG2 on the silica support under varying solvent and substrate concentrations.

Ten green pellets of HG2/silica gel were placed in a glass vial and one unloaded white pellet of silica gel was added. Three identical sets of such eleven pellets were brought into contact with a 5 ml toluene solution (A), a substrate mixture of 0.05 M *cis*-cyclooctene in hexane (B), and a concentration of 0.8 M *cis*-cyclooctene in hexane (C), respectively. After 4 hours of shaking and solvent evaporation, vial A contained 11 coloured pellets, whereas vial B and C contained one unloaded white pellet next to ten green pellets. In other words, HG2 leaches from the silica support in toluene and is redistributed among the eleven pellets. Under apolar conditions (hexane), and

View Article Online
DOI: 10.1039/C5CY01897H

Table 1. Characterization of the supports and activity of the immobilized catalysts.

Entry	Material	Ru (wt%)	Split test[e]	$D_{particle}$ (μm)[f]	D_{meso} (nm)[g]	Morpho-logy	Pore architecture	V_{meso} ($cm^3\ g^{-1}$)	V_{micro} ($cm^3\ g^{-1}$)	BET ($m^2\ g^{-1}$)	TOF_i ($s^{-1}.10^{-2}$)
1	HG2[c]	-		-	-	-	-	-	-	-	13
2	Silicalite-1	0.008	-	-	0.54	Coffin	MFI topology	-	-	350	-
3	$AlPO_4$-5	0.001	-	-	0.73	n.d.	AFI topology	-	-	-	-
4	Si-VPI-5	0.12	-	-	1.1	Needles	VFI topology	-	-	-	-
5	Silica Gel[a]	0.35	+	2000	n.d.	Irregular	Non-ordered	n.d.	n.d.	375	4
6	Silica Gel[b]	0.30	+	50	6	Irregular	Non-ordered	0.72	0	406	4.5
7	KIT-5	0.35	+	10-25	7[d]	Irregular	Cubic *Fm3m*	0.30	0.37	1054	1.5
8	SBA-16	0.16	+	4-25	5.5[d]	Irregular	Cubic *Im3m*	0.14	0.17	535	2
9	SBA-15	0.29	+	2-5	10	Fibre-like	Hexagonal *p6mm*	0.98	0.12	791	3
10	SBA-3	0.28	+	1-5	1.8	Platelets	Hexagonal *p6mm*	0.68	0	1476	3
11	KIT-6	0.26	+	2-5	6	Irregular	Cubic *Ia3d*	0.72	0.13	700	5
12	MCM-48	0.26	+	0.3-0.7	2.5	Sphere	Cubic *Ia3d*	0.72	0	1600	5.5
13	SBA-15	0.34	+	0.5-1	5.5	Rope-like	Hexagonal *p6mm*	0.51	0.51	1097	8
14	C12-MCM-41	0.24	+	0.3-0.5	2.6	Sphere	Hexagonal *p6mm*	0.34	0	690	8.5
15	C16-MCM-41	0.29	+	0.3-0.5	3.3	Sphere	Hexagonal *p6mm*	0.67	0	1333	8.5
16	C18-MCM-41	0.33	+	0.3-0.5	3.6	Sphere	Hexagonal *p6mm*	0.85	0	1446	7.5
17	TUD-1	0.21	+	5-20	8-15	Irregular	Disordered	1.1	0.04	417	10

[a] Grace Silica Gel 239 pellets; [b] Silica Gel 60 (Davisil Grade); [c] 0.33 mol% HG2 compared to *cis*-cyclooctene; [d] pore entrance diameter (cage diameter not experimentally determined: KIT-5[77] = 6.8-8.3 nm and SBA-16[82] =5.1-7.2 nm). [e] – split: homogeneous activity; + split: heterogeneous activity. Reaction conditions: 0.05M *cis*-cyclooctene; 5 mL hexane; 50 mg HG2/ support (pretreated at 150 °C); 35 °C. The homogeneous reaction (entry 1) is performed in toluene instead of hexane for solubility reasons. [f] $D_{particle}$ = particle diameter. [g] D_{meso} = mesopore diameter. [h] Error in TOF_i determination is < 0.5 $s^{-1}.10^{-2}$.

independent of substrate concentration, HG2 remains anchored on the support as no migration was observed throughout the liquid reaction mixture. Physisorption of HG2 on silica is thus truly heterogeneous, provided that the solvent is apolar with restricted solubility of HG2.

Stability of the immobilized catalyst – A continuous experiment

The experiment in Figure 2 already showed a firm anchoring of HG2 on silica support under reaction circumstances, but a continuous experiment is a better measure of catalyst robustness. For the actual experiment, 110 mg of a 0.20 wt% Ru loaded HG2/TUD-1 (pellets) were packed in a reactor together with quartz-wool and glass beads. The catalyst bed had dimensions of 0.94 x 3.5 cm. A solution of 0.4 mol L^{-1} *cis*-cyclooctene in hexane was pumped through the reactor at room temperature dosed at 38 mL $g_{cat}^{-1}\ h^{-1}$. The reactor outlet was sampled at regularly times. The accumulated turnover number (TON) is represented in Figure 3.

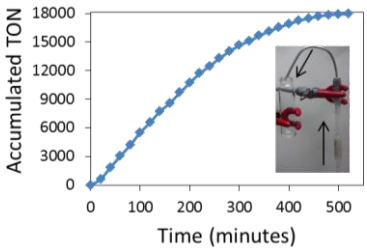

Figure 3. Accumulated TON in a continuous experiment of HG2/ TUD-1. To the right, the set-up of the reaction with the direction of the feed flow.

Initially, about 40 % cyclooctene is converted, but the conversion decreases to 25 % after 200 min. and faded to 3 % at the end of the reaction after 540 min. At this point, a TON of 18000 was obtained, corresponding to a conversion of 39 gram cyclooctene per gram catalyst. To the best of our knowledge, this is the highest reported TON for the ROMP of non-purified *cis*-cyclooctene under ambient conditions with an immobilized HG2 complex.

Thermal treatment of the support

Surface hydroxyl groups were reported essential to anchor HG2, but this was not investigated.[58] Thermal treatment of silica materials removes physisorbed water molecules from the surface and changes the chemical composition by a surface dehydroxylation process forming siloxane moieties.[83] If surface hydroxyls are important in HG2 immobilization, thermal treatment of the parent support material should have a substantial influence on catalyst immobilization. Therefore, prior to HG2 immobilization, MCM-41 (3.3 nm pores) and TUD-1 were subjected to elevated temperature treatments, ranging from 150 °C to 900 °C. Samples without treatment, kept at 25°C, were used as a reference. The immobilization process was conducted under identical conditions as before. The initial activities of variously pre-treated HG2/TUD-1 and HG2/MCM-41, measured as TOF_i, in metathesis of *cis*-cyclooctene are compared in Figure 4. The corresponding kinetic profiles, plotting conversion in time, are shown in the supporting information (Figure S3 and S4). Thermally treating MCM-41 leads to a higher activity, the TOF_i increasing with elevating temperature. The activity gain is most pronounced after heating at 150°C, while a further gradual increase is observed up to 700°C. Overall, the TOF_i increases from 2.5 $s^{-1}.10^{-2}$ for the untreated up to 10.5 $s^{-1}.10^{-2}$ for the 700 °C treated MCM-41. Treatment at 900 °C also lead to an active catalyst, however considerable Ru leaching into solution is observed with this catalyst. The same trend is observed for TUD-1, though the preferred treatment here is below 400 °C. Higher treatment temperatures for TUD-1 led to inferior catalytic results, accompanied by a fast green-to-brown coloration of the

catalyst. A spectroscopic study was performed to rationalize these thermal treatment effects.

The temperature-induced dehydration and dehydroxylation of the silica surface was therefore monitored by (near) infra-red (IR) spectroscopy by changes in the ν_{O-H} vibration (3800-3000 cm^{-1}) and $(\nu+\delta)_{O-H}$ (4800-4200 cm^{-1}) overtone domain at different temperatures. The data of the IR spectroscopic study are collected in Figure S5.

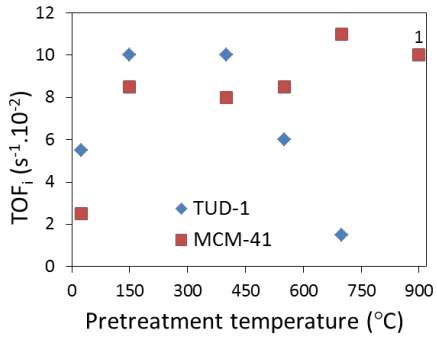

Figure 4. Influence of a thermal treatment of the support on the TOF_i of HG2/TUD-1 (0.21 wt% Ru) and HG2/MCM-41 (0.30 wt% Ru). [1]This sample shows considerable Ru leaching, therefore overestimating the contribution of heterogeneous TOF. Reaction conditions: 0.05 M *cis*-cyclooctene; 5 mL hexane; 50 mg HG2/support; 35 °C.

Quantification of the silanol density was accomplished by integrating the $(\nu+\delta)_{O-H}$ absorption bands, as the molar integrated absorption coefficient of these bands $\varepsilon_{(\nu+\delta)O-H}$ does not vary with the nature and concentration of silanol groups.[84] At room temperature the surface is completely hydroxylated, together with a monolayer of physically adsorbed water, while drying the support at 150 °C and atmospheric pressure (or 50 °C under vacuum) removes the hydrogen-bonded water and leaves the hydroxyl groups intact. At higher temperature treatments, geminal and vicinal silanols gradually disappear in favour of isolated silanols and surface siloxanes.[83] The silanol density per gram of TUD-1 and MCM-41 together with the ratio of silanol density per surface area, of the two catalysts, i.e. TUD-1 to MCM-41, are represented in Table 2.

Table 2. Silanol densities (mmol OH g^{-1}) of TUD-1 and MCM-41 after pretreatment at elevated temperatures.

	25 °C (mmol OH g^{-1})	150 °C (mmol OH g^{-1})	400 °C (mmol OH g^{-1})	550 °C (mmol OH g^{-1})	700 °C (mmol OH g^{-1})
TUD-1	1.30	1.27	0.74	0.53	0.48
MCM-41	4.35	4.35	3.22	2.34	1.59
TUD-1: MCM-41[a]	0.96	0.93	0.73	0.73	0.96

[a]ratio OH density of TUD-1:MCM-41 (calculated in mmol.m^{-2}). TUD-1: 417 m^2 g^{-1}; MCM-41: 1333 m^2 g^{-1}.

The silanol density per surface area of the parent material is comparable for the two silica materials and corresponds to 2 OH per square nm, which is in accord with literature.[83] As expected, the silanol density remains intact after heating until 150°C, but decreases with elevating temperature, albeit differently for both silicas. Considering the potential anchoring role of silanols, a plot of the total silanol density per Ru site against the initial activity of HG2/TUD-1 and HG2/MCM-41 was constructed in Figure 5. Untreated materials TUD-1 (25°C; with 63 OH per Ru) and MCM-41 (25°C; with 145 OH per Ru) are represented by the blue dots and contain physisorbed water. Dehydration of these materials at 50 °C under vacuum (at 10 mbar) or at 150 °C (at atmospheric pressure) removes this water, but retains the chemisorbed silanols. The chemical equivalence of these two treatments was confirmed by NIR diffuse reflectance spectroscopy (Figure S6).[85] As this dehydration step led to the sharpest activity increase, as visualized by the blue arrows in Figure 5, presence of water is clearly disadvantageous for metathesis catalysis, but also, it can be concluded that the type of silanol is less crucial for the catalytic activity. As the observation of the typically green colour indicates a stable HG2 on the untreated supports, their lower activity is not caused by catalyst deactivation, but rather polarity effects, retarding *cis*-cyclooctene diffusion in pores filled with water is the cause of the slow catalysis. In fact, it may be estimated by TGA and surface area measurements that water covers about 20 % and 60 % of the mesopore surface of MCM-41 and TUD-1, respectively.

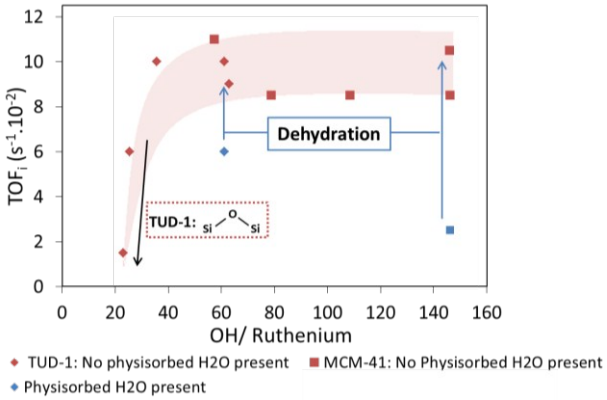

Figure 5. Influence of molar ratio of silanols to Ru on the initial activity of the ROMP of *cis*-cyclooctene when physisorbed water is present (blue dots), or with a fully dehydrated support (red dots). Reaction conditions: 0.05 M *cis*-cyclooctene; 5 mL hexane; 50 mg HG2/MCM-41 and TUD-1 (pre-treated at different temperatures; loading of 0.30 wt% Ru for HG2/MCM-41 and 0.21 wt% Ru for HG2/TUD-1); 35 °C.

Experimental verification of the water effect is accomplished by intentionally adding the amount of water, that is removed by the thermal treatment from 25 °C to 150 °C, to a water-free HG2/MCM-41 catalyst (pre-dried at 150°C). Addition of water indeed lowered the TOF_i from 8.5 $s^{-1}.10^{-2}$ to 6.0 $s^{-1}.10^{-2}$ in accord to the above considerations. The red dots in Figure 5 represents the activity of thermo-treated HG2/TUD-1 and HG2/MCM-41. The thermal treatment was varied between 50 °C (10 mbar vacuum) and higher temperatures (atmospheric pressure). From the right to the left hand-side, the silanol density decreases as a consequence of a dehydroxylation process. Clearly, high activities are observed as soon as water is removed, leaving sufficient content of silanols, *viz*. at least more than 40 OH per Ru. Treating the parent TUD-1 sample at temperatures higher than 400 °C substantially reduces the catalytic activity, whereas a treatment of the MCM-41 support

at 900 °C led the catalytic activity unchanged, albeit accompanied with considerable complex leaching in the latter case. Neither of the two phenomena originate from a temperature-induced collapse of the pore structure, as N_2 physisorption proved an intact structure for TUD-1 treated at 700 °C and the characteristics of MCM-41 mainly remained unchanged up to 900 °C (although some pore shrinkage occurred at 900 °C) (Table S1), in accord with literature-reported data of Si-MCM-41 under the same heating conditions.[86] As the decrease in activity for HG2/TUD-1 at 400°C treatment is accompanied by a rapid green-to-brown colour change, we hypothesized that the presence of strained siloxane bridges causes catalyst deactivation. Such reactive siloxanes have indeed been described as reactive sites on silica surfaces in different reactions[87, 88], as well as being responsible for decomposition of Ru complexes due to Ru-O-Si bond formation.[76] The concentration of such siloxanes typically increases with rising of the pretreatment temperatures, but why the observed catalyst deactivation is only prominent for TUD-1 is unclear. As a difference in siloxane reactivity may explain this phenomenon, the presence and reactivity of siloxanes were monitored.

An easy chemical method to determine the strained siloxanes involves its reaction with NH_3 under continuous flow at elevated temperature to form Si-NH_2, after passivating the reactive surface hydroxyl groups with dichlorodimethylsilane (DCDMS).[89-91] Finally, hydrolysis of the unstable Si-NH_2 in water, forming a silanol and ammonia, and measuring of the pH allows a good estimate of the reactive siloxanes. The chemical surface transformations during the procedure were monitored with FT-IR spectroscopy (Figure 6).

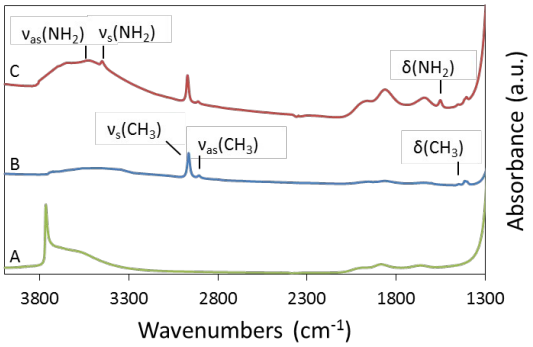

Figure 6. IR spectra of A: TUD-1 treated at 150 °C; B: TUD-1 after passivation with DCDMS; C: TUD-1 after passivation with DCDMS and reaction with NH_3.

TUD-1, pretreated at 150 °C, shows an intense vibration band at 3745 cm^{-1} (ν_sOH) and a broad shoulder at lower wavenumbers due to hydrogen bonding phenomena (Figure 6A). After treatment with DCDMS, the 3745 cm^{-1} band completely disappears at the expense of three new features at 2970, 2901 and 1460 cm^{-1}, corresponding to $\nu_s(CH_3)$, $\nu_{as}(CH_3)$ and $\delta(CH_3)$ respectively (Figure 6B).[92] Ammonia reaction with siloxanes is evidenced by the characteristic absorption at 3536, 3452 and 1550 cm^{-1}, attributed to $\nu_{as}(NH_2)$, $\nu_s(NH_2)$ and $\delta(NH_2)$ vibrations, respectively (Figure 6C).[93] Subsequent hydrolysis and pH measurements allows determination of the reactive siloxane content. The amount of ammonia recuperated per gram catalyst, as a measure of Si-NH_2, as well as the corresponding number of siloxanes and the average distance of silanols on the surface of TUD-1 and MCM-41, are presented in Table 3. TUD-1, though treated at lower temperature (here: 550°C), shows a substantial amount of strained siloxanes, whereas their abundancy is ten times less, even for a 900°C treated MCM-41 sample. The high content of reactive siloxanes on TUD-1 may therefore be considered to cause deactivation of HG2. Though the thermally treated MCM-41 being free of siloxanes, keeps HG2 intact in accord with its green colour, the treatment at 900°C causes considerable leaching of the Ru complex. The lower affinity to HG2 is likely due to the lesser amount of remaining silanols, isolated at too large distance from each other (2.5 nm).

Table 3. NH_2 contents on TUD-1 and MCM-41.

	NH_3 reacted (mmol g^{-1})	Siloxanes[a] (% as OH)	Distance silanols (nm)
TUD-1 (550 °C)	0.048	3.8	1.3
MCM-41 (900 °C)	0.0037	0.1	2.5

[a] siloxanes reacted with NH_3 divided by total silanol density.

In conclusion, for stable metathesis with supported HG2, the mesoporous silica should be treated at elevated temperatures, preferably for MCM-41 and TUD-1 at 50 °C under vacuum (10 mbar) or at 150 °C under atmospheric pressure, prior to immobilization, to remove physisorbed water and to conserve a high amount of silanol anchors for immobilization. Therefore, care has to be taken to prevent formation of reactive siloxane bridges during thermal treatment of the support as to keep the surface unreactive toward HG2. Remarkably, the necessity of silanol groups for stabilization of HG2 is in contrast with previous studies that reported the detrimental role of silanol groups on the stability of the Grubbs 1st generation complex.[50, 76, 94]

Adsorption isotherms of HG2 on mesoporous silica

As a high affinity of the support for HG2 is desirable to prevent decomposition and leaching, adsorption isotherms of HG2 for 150°C dried MCM-41 (3.3 nm pores) and TUD-1 were determined and investigated (Figure 7). A raise of HG2 concentration in the sorption solution initially results in a linear increase of immobilized HG2 (Figure 7A), whereby 4 out of 5 HG2 molecules adsorb from the solution on the support, with an adsorption rate of 4 µmol HG2 per gram per minute. This corresponds to 1 and 3 µmol HG2 per mmol OH per minute for MCM-41 and TUD-1, respectively. At higher concentrations, higher loadings are observed on MCM-41 compared to TUD-1, which is in line with the higher surface area and thus anchoring capacity of MCM-41 per silica weight. A sharp deflection from linear uptake is observed for both TUD-1 and MCM-41 at Ru equilibrium concentrations above 0.7 and 1.7 mM, respectively, the adsorption process becomes thus less efficient at higher HG2 concentrations. Though pore blockage by HG2 itself cannot be excluded as explanation for

View Article Online
DOI: 10.1039/C5CY01897H

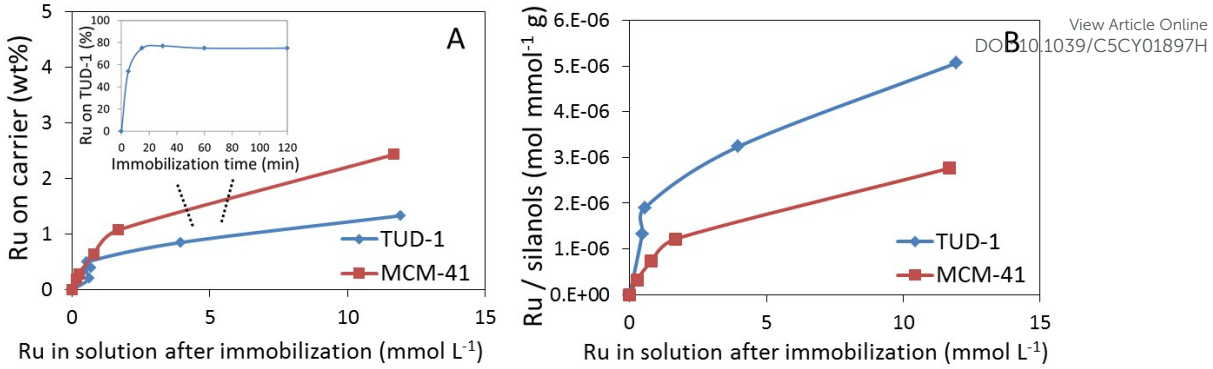

Figure 7. A) Carrier loading (wt%) of Ru on TUD-1 and MCM-41 at different concentrations of HG2 in toluene. The kinetic profile of immobilization is presented in the inset. For both materials the adsorption equilibrium was reached after 30 minutes, and therefore the adsorption isotherm experiments were run for 45 minutes to obtain thermodynamically sound HG2 uptake values. B) Modified adsorption isotherms of Ru on TUD-1 and MCM-41. Both supports are pre-treated at 150 °C prior to immobilization.

the decreasing uptake efficiency with increasing HG2 loading, the sharp distinctive shape of the isotherm of both materials rather points to the existence of two distinct adsorption sites, one with high affinity (occupied at low loadings) and the other with low affinity for HG2 (at higher catalyst loadings). In the modified adsorption isotherm (Figure 7B) the uptake profile of HG2 is normalized for the amount of silanols (and at the same time for the surface area as MCM-41 and TUD-1 have equal surface silanol densities of 0.003 mmol m^{-2}), rather than for the weight of catalyst. The deflection of the affinity sets in at $8.2.10^{-5}$ and $1.2.10^{-4}$ mmol HG2 m^{-2} ($1.22.10^{-6}$ and $1.90.10^{-6}$ mol HG2 $mmol^{-1}$ OH g) for MCM-41 and TUD-1, respectively, corresponding to 1.1 wt% Ru for MCM-41 and 0.5 wt% Ru for TUD-1. The total adsorption capacities at room temperature were estimated to be 3.2 and $1.8.10^{-4}$ mmol HG2 m^{-2} for TUD-1 and MCM-41, respectively.

Since both TUD-1 and MCM-41 materials show a comparable OH surface density (Table 2), a difference in surface uptake behaviour of the respective silica was not expected. The plot nevertheless reveals a higher affinity of the TUD-1 silica surface and thus thermodynamically more favourable adsorption sites are present when compared to that of MCM-41. ^{29}Si MAS NMR of the surface of both support materials, pretreated at 150 °C, was therefore studied. By distinguishing the signal for isolated and geminal silanols, according to Ide *et al.*[95], clear structural differences were observed: 150°C treated TUD-1 has a substantially higher fraction of geminal silanols (Q_2/Q_3+Q_2= 0.19) compared to similarly dried MCM-41 (Q_2/Q_3+Q_2= 0.10), suggesting that HG2 more favourably interacts with that silanol type. The amount of geminal silanols exceeds the linear uptake of HG2 with a factor 5 for TUD-1 and 3.5 for MCM-41, which corresponds to a higher density of 5.7 $.10^{-4}$ mmol m^{-2} TUD-1 compared to 3.1 $.10^{-4}$ mmol m^{-2} on MCM-41. Awaiting for additional arguments for the (enthalpic) difference in surface adsorption chemistry, steric (entropic) factors due to space restrictions, most pronounced in the smaller pores of MCM-41, cannot be excluded.

Influence of active site density on catalytic activity

Heterogeneous metathesis reactions are preferably carried out with highly loaded HG2 complex, as long as HG2 instability and pore diffusion limitations (PDL) are absent. The optimal active site density was therefore searched for by systematically increasing HG2 loadings, ranging from 0.1 to 2.5 wt% Ru, on 150°C dried MCM-41 (3.3 nm pores) and TUD-1. The total catalyst weight in the catalytic tests remained constant (50 mg). All immobilized catalysts were bright green and thus not affected by deactivation. Whereas both supports show increasing conversion rates with higher HG2 loadings (Figure S7), the activity per catalytic complex (TOFi), as shown in Figure 8, indicates a more steep decrease of the TOFi for HG2/MCM-41. Such behaviour is less obvious for HG2/TUD-1 as only a slight drop of the TOFi to 9 s-1.10-2 is observed at 1 µmol HG2, corresponding to 2.1 wt% Ru.

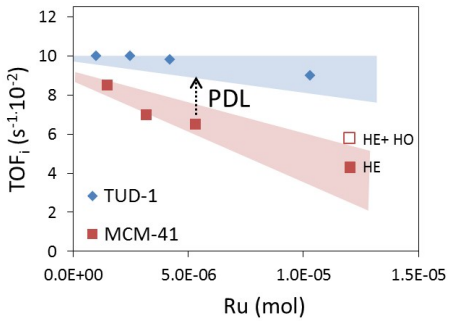

Figure 8. Influence of the abundance of ruthenium per catalyst volume on the initial activity (TOF_i). PDL= pore diffusion limitations. HE= heterogeneous activity; HO= homogeneous activity. Reaction conditions: 0.05 M *cis*-cyclooctene; 5 mL hexane; 50 mg HG2/TUD-1 or HG2/MCM-41 (pre-treated at 150 °C); 35 °C.

Therefore, loadings up to 2 wt% are possible on TUD-1 without losing catalyst efficiency. Indeed, the experimental verification, where the TOF_i is compared between two reactions with catalysts having a different catalytic loading, is called the Koros and Nowak criterion. According to this criterion, PDL is excluded whenever the turnover frequency is invariant of the density of the active sites.[96] This criterion is only valid under the following conditions: 1) isothermal reactions with negligible thermal gradients; 2) every added catalytic complex should be identical to the previous one and represent one catalytic site.[97] As these conditions are satisfied in our work, the rate of cyclooctene metathesis with HG2/TUD-1 up to 2 wt% Ru is determined by the catalytic reaction and not by

mass transport. Higher loadings though will render the catalysis inefficient due to PDL and thus artificial underestimation of TOFs.

HG2/MCM-41 has a more steep activity decrease from 8.5 $s^{-1}.10^{-2}$ at 1.5 µmol HG2 (0.30 wt% Ru) to 6 $s^{-1}.10^{-2}$ at 12 µmol HG2 (2.4 wt% Ru), and seems thus more susceptible to mass transport phenomena than HG2/TUD-1. In fact, this conclusion is in line with the smaller pore size of MCM-41 (3.3 nm) compared to that of TUD-1 (8-15 nm). The decrease in activity could be attributed to a lower effective cyclooctene concentration in the pores leading to a lower activity on one hand, or to a less accessible active Ru site caused by pore obstruction on the other hand. The true mechanism behind this activity decrease was unravelled by carefully investigating product selectivity and will be discussed in the next paragraph.

Note that extrapolation of the catalytic activity towards low Ru loading, thus free of PDL, shows fairly similar TOFs irrespective of the mesoporous silica type, the value being close to that of the homogeneous HG2 catalyst. This means that despite dissimilarities of affinity and precise anchoring of HG2, no essential impact on the catalytic activity between the two supported HG2 catalysts is observed.

The original activity of the highly loaded HG2/MCM-41 (2.4 wt% Ru) on the graph in Figure 8 seems erroneous, as a TOF well below the observed 6 $s^{-1}.10^{-2}$ was expected due to PDL contribution. A split test and ICP-AES analysis of the reaction solution pointed to significant leaching of HG2 for this highly loaded MCM-41. Subtracting the homogeneous activity of HG2 gives a true heterogeneous contribution (HE) of 4.3 $s^{-1}.10^{-2}$; which better fits the expectations. Besides confirming mass transfer issues with MCM-41, this experiment shows that stably anchoring of high HG2 loadings are better accomplished on TUD-1.

Kinetic dissimilarities between supported and non-supported HG2

The enthalpic driving force of cyclic molecules like cyclooctene enables them to undergo irreversible ROMP metathesis, thereby releasing ring-strain. The formation of linear polymers is therefore accompanied by the formation of low-molecular-weight cyclic oligomers, which originates from the direct cyclo-oligomerization of cyclooctene or from polymer back-biting.[98] The final ring-chain equilibrium is, besides the catalyst and ring-strain of the cycloolefin, mostly dependent on the monomer concentration.[99, 100] In 1950, Jacobson and Stock-mayer (J-S) developed a theory of ring-chain equilibria, including a prediction of the statistical distribution of cyclic structures at equilibrium. While at low monomer concentrations mostly cyclic oligomers are formed, linear polymers are formed at high concentrations. The highest concentration whereby no linear polymers were formed at equilibrium situation was defined as the critical monomer concentration.[101] This model was later refined by Kornfield et al., taking into account the ring-strain phenomenon, which was neglected in the J-S theory.[102] (For further theoretical background, see supp. info). The critical concentration $[M]_{c,\infty}$ was hereby calculated to be 0.21 mol/L for cyclooctene, as in agreement with experimental data. Thus, at concentrations lower than 0.21 M, mostly cyclic oligomers are formed in presence of homogeneous metathesis catalysts. The successful employment of the homogeneous HG2 complex for the formation of a library of macrocycles was already demonstrated multiple times in literature.[103-105]

From our interest in selectively synthesizing cyclic oligomers, we evaluated this reaction at low monomer concentrations with a homogeneous HG2 catalyst and compared the catalytic outcome (product selectivity) with that of a reaction in presence of the immobilized complex on porous silica under batch conditions. The potential of this reaction was proposed earlier by us[106] and later by research groups centred around BASF[66] and described under continuous-flow conditions.[60] As heterogeneous reactions are often confronted with confinement and diffusion issues, kinetic dissimilarities between homo- and heterogeneous metathesis catalysed reactions may be expected.[107] This will especially be likely when linear oligomeric and polymeric products are involved in heterogeneous ROMP reactions. Careful product analysis was therefore attempted during the metathesis of cyclooctene in presence of homogeneous HG2 and HG2/MCM-41 (3.3 nm pores; 0.30 wt% Ru). Cyclic oligomers up to the pentamer (C40) were analysed with GC, whereas the larger non-volatile macrocycli (C48-C56) together with linear oligomers and polymers were monitored by GPC to complete the mass balance. The molecular weight range of these fractions is provided in the method section (catalytic reactions) and extra information about GPC analysis is reported in the supporting information (Figure S8).

The experimental results of a homogeneous reaction (0.05 M *cis*-cyclooctene) are presented in Figure 9. At low cyclooctene conversion, mostly linear oligomers and small cyclic oligomers are formed with a minor amount of linear polymer. As the reaction proceeds, the linear polymer and oligomer fraction is converted almost exclusively to cyclic oligomers (Figure 9A). Extrapolation of the initial development of the reaction to zero conversion indicates that linear polymerization largely overrules the initial direct formation of cyclic oligomers from cyclooctene (Figure 9A and B). The cyclic oligomers are predominantly formed through back-biting of the growing linear oligomer and polymer chains which, once formed, are quickly converted. This kinetic reaction pattern was similar to the ones observed with Grubbs II and Grubbs-Nolan catalysts.[104] The cyclic oligomer fraction maximizes at 46 % conversion (selectivity of 98 %), and the selectivity decreases only slightly to 94 % at full conversion in favour of larger cyclic oligomers (4 %) and linear oligomers (2 %) upon reaching thermodynamic equilibrium (Figure 9B). The majority of the cyclic fraction consists of C16-C56 cyclic oligomers and the weight distribution is given in Figure 9C, which was consistent with equilibrium distributions obtained by different authors.[60, 104, 108] The observed equilibrium ring distribution was compared to the one predicted by the original J-S theory, as indicated by the black bullet points in Figure 10C, which foresees a decrease of the molar cyclic oligomer concentration C_i (with degree of polymerization *i*) with increasing ring size

View Article Online
DOI: 10.1039/C5CY01897H

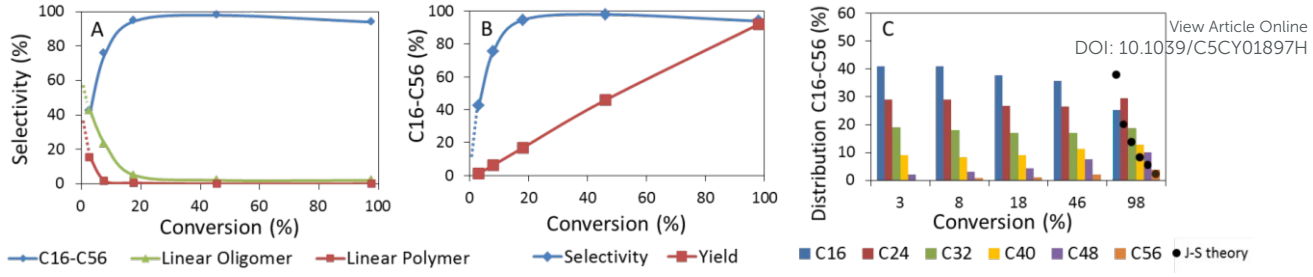

Figure 9. Homogeneous RO-RCM with *cis*-cyclooctene. A) Distribution of the cyclic oligomer/ linear oligomer/ linear polymer fraction in function of conversion. B) Yield and selectivity of C16-C56 with increasing conversion. C) Distribution (wt%) of C16-C56 cyclic oligomers. Reaction conditions: 0.05 M *cis*-cyclooctene; 16 mL toluene; 3 mg HG2; 35 °C.

proportional to $i^{-5/2}$.The equilibrium distribution observed here clearly does not obey this theory, since the dimer C16 is overestimated and its concentration (on weight base) is surpassed by the trimer C24, likely due to enthalpic reasons as C16 has a higher ring-strain compared to C24 (which is neglected in the J-S theory).[102] Furthermore the proportion of larger cyclic oligomers exceed the predicted values. Based on the experimental data, relative molar equilibrium constants K_i for cyclic oligomers with a degree of polymerization *i* were determined and compared to those obtained by the J-S theory and the refined model of Kornfield and coworkers (Figure S9). For cyclic oligomers larger than the trimer C24, the predicted slope of -2.5 is well approximated; the deviation of K_i from theoretical values is larger for smaller cycles.

The reaction was performed as well at other monomer starting concentrations. At low concentrations, *i.e.* 0.025 and 0.1 M, C16-C56 cyclic oligomers are formed almost exclusively at equilibrium, reaching 99 and 91 % product selectivity, respectively. At higher concentrations (0.3 M), this fraction drops to 65 %, which is reasonable since the initial monomer concentration exceeds the critical concentration of 0.21 M. A graphical representation of this ring-chain equilibrium at different concentrations is shown in Figure S10. The distribution within the C16-C56 cyclic oligomer fraction seems also related to this critical concentration. The results are presented in Table 4. At concentrations below [M]c,∞, ring distributions are identical, while at 0.3 M, larger cyclic oligomers (C40-C56) are more prominent. This is due to the fact that the critical concentration of cyclic oligomers increases proportional to their ring size.[109]

Table 4. C16-C56 cyclic oligomer distribution at equilibrium starting from different *cis*-cyclooctene concentrations.

	C16	C24	C32	C40	C48	C56
0.025 M	25	29	20	14	8	4
0.05 M	25	30	20	14	8	4
0.1 M	23	28	20	14	10	5
0.3 M	18	25	20	17	13	6

Reaction conditions: 0.025–0.3M *cis*-cyclooctene; 16 mL toluene, 3 mg HG2; 35°C.

At low conversions, the effect of concentration on the product distribution is even more outspoken. While at low monomer starting concentrations cyclic oligomers are predominantly formed through backbiting of (long) linear chains, as indicated for 0.05 M in Figure 9A and B, the initial cyclic oligomer concentration decreases at higher concentrations. For instance, at a cyclooctene conversion of 5 %, the selectivity towards cyclic oligomers decreases from 54 % at 0.025 M, to 39 % for 0.1 M and 26 % for 0.3 M, in favour of (long) linear chains (Figure S11A). As polymer growth is depending on monomer concentration, in contrast with polymer back-biting, which is the main route to cyclic oligomers under these reaction conditions, it is conceivable that a higher monomer concentration leads to a higher degree of polymerization initially. Moreover, the lower the initial monomer concentration, the higher the probability of a direct cyclic oligomer formation. The ratio between the C16-C56 fraction likewise changes with increasing monomer concentration. In particular, the contribution of C40-C56 cyclic oligomers increases (at 5% conversion) (Figure S11B). Although the selectivity towards C16-C56 is lower at higher concentrations (0.1 and 0.3 M), its molar concentration is still higher compared to *e.g.* 0.05 M., enhancing the self-metathesis of cyclic oligomers (C16+16=C32 or C16+C24=C40), thus affording C40-C56-enriched concentrations.

Impacting the kinetic product distribution is not limited to variation of the feed concentration, as the catalyst itself may also contribute hereto. Kavitake *et al.* showed that with an unsymmetrical NHC-modified catalyst a 2:1 ratio of C16:C24 could be obtained at low conversions, attributed to the dual-site configuration of the homogeneous catalyst.[104] Depending on the steric confinement, the active catalyst selectively discriminates between ring-closing and propagation. After 30 % conversion of 0.025 M cyclooctene, C16 and C24 are formed with 57 and 27 % selectivity, respectively, while our observed ratio of C16:C24 is much lower (1.5:1) at 20 % conversion of 0.025 M cyclooctene with the symmetrical HG2 catalyst.

The homogeneous conversion of the RO-RCM of cyclooctene was compared to a heterogeneous reaction with HG2/MCM-41 (0.30 wt% Ru), as displayed in Figure 10. Initially, linear oligomers and polymers are formed next to a large fraction of C16-C56 cyclic oligomers (Figure 10A). Compared to the unsupported HG2, a higher initial C16-C56 selectivity was obtained (56 % at a conversion of < 2%). As the reaction proceeds, the linear polymer fraction reaches a maximum of 25 % at 33 % conversion and undergoes further back-biting to cyclic oligomers at prolonged reaction times. At full conversion, the reaction mixture comprises 87 % of C16-C56 cyclic oligomers and 8 % of linear oligomers (mass balance of 95 %), while larger cyclic oligomers (> C56) were neglected because of their low abundance. The larger fraction of linear

View Article Online
DOI: 10.1039/C5CY01897H

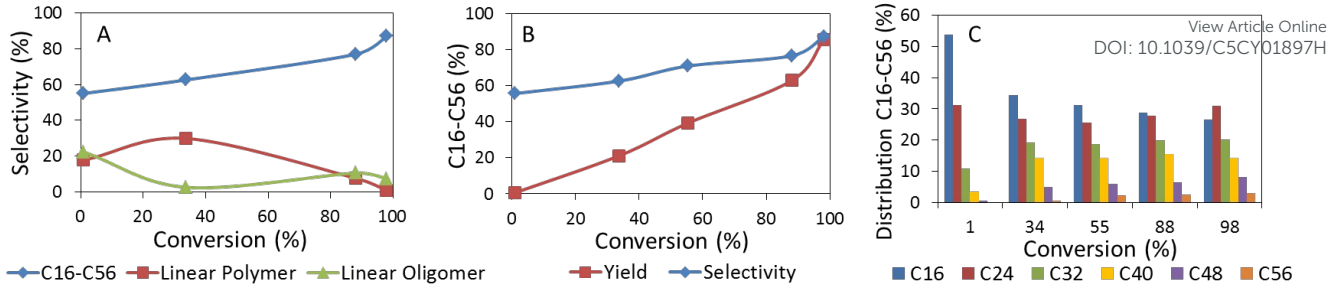

Figure 10. Reaction profile of a heterogeneous RO-RCM with *cis*-cyclooctene with HG2/MCM-41. A) Distribution of the cyclic oligomer/ linear oligomer/ linear polymer fraction in function of conversion. B) Yield and selectivity of C16-C56 with increasing conversion. C) Distribution of C16-C56 cyclic oligomers (wt%). Reaction conditions: 0.05 M *cis*-cyclooctene; 16 mL hexane; 160 mg HG2/MCM-41 (pretreated at 150 °C; 0.30 wt% Ru); 35 °C.

oligomers in presence of the supported HG2 at equilibrium situation, *viz*. 8 % *vs.* 2 %, could be ascribed to secondary intermolecular chain transfer reactions. Hereby a rearrangement of double bonds occurs between two different nearby growing polymer chains, a phenomena that seems plausible in the pores of a heterogeneous catalyst where adjacent Ru-polymer chains can interact closely.[110] The previous observations though were surprising as the formation of linear polymers was not reported in earlier studies with heterogeneous ROMP of cyclooctene, neither was this observed in that extent in our homogeneous reaction.[59, 60] These results do however demonstrate the potential of heterogeneous metathesis in depolymerization reactions of *e.g.*, polybutadiene to multiple unsaturated macrocycles. Figure 10B displays the yield and selectivity to the cyclic fraction in function of time, while the product distribution within the C16-C6 fraction is presented in Figure 10C. Although the distribution practically equals the one of the homogeneous reaction, the contribution of C48 is slightly higher homogeneously. A molar ratio of C40:48 of 1.3 was obtained with the soluble HG2, and increased to 1.8 in presence of the supported HG2.

Most outspoken dissimilarities between the homo- and heterogeneous catalysed reaction, *i.e.* the higher initial C16-C56 cyclic oligomer selectivity and the presence of linear polymer up to 25 %, are derived from the peculiar metathesis catalysis occurring in the pores of the catalyst. Diffusion problems of cyclooctene into the pores (*vide supra*, Figure 8) lead to a lower effective cyclooctene concentration in the pores, stimulating the direct formation of cyclic oligomers instead of linear chains. The C16-C56 fraction reaches therefore a higher initial selectivity of 60 % (5 % conversion) in comparison with the unsupported HG2. The presence of diffusion problems of cyclooctene into the pores implies that the same is valid for the diffusion of products out of the pores into the bulk. As a result, the formed cyclic oligomers tend to react further to linear oligomers and polymers. Indirect formation of cyclic oligomers through back-biting is hindered due to pore confinement effects and the linear chains accumulate in the pores.

Pore diffusion also creates a product shift within the C16-C56 cyclic oligomer fraction. The difficult diffusion of cyclooctene (C8) in and the diffusion of larger cyclic oligomers out of the pores induces a lower C8:C16 ratio inside the pores. As a consequence, C16 cyclic oligomers tend to undergo self-metathesis, forming C32 (schematic representation in Figure S12). A higher C32:C24 ratio is thus expected and also observed with the immobilized catalyst, as supported by the data in Figure 11.

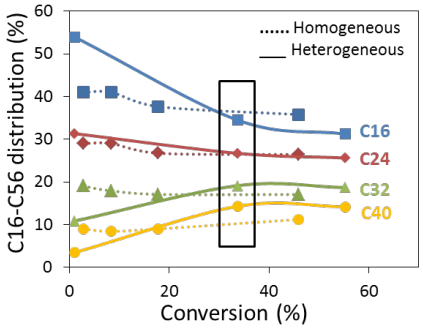

Figure 11. Distribution of C16-C40 cyclic oligomers for a homogeneous and heterogeneous catalysed metathesis of *cis*-cyclooctene (0.05 M). Reaction conditions: See Figure 9 and Figure 10.

These kinetic differences between homo- and heterogeneous HG2 catalysis disappear at full conversion as to obey the thermodynamic equilibrium distribution.

The equilibrium situation attained with HG2/MCM-41 was further compared with the homogeneous reaction at different concentrations. Overall, a lower selectivity towards the cyclic C16-C56 fraction is attained at equilibrium with the supported HG2, in favour of linear oligomers, which is clearly visible in Figure 12. (Eq. distribution of cyclic oligomers in Figure S13). While at 0.025 and 0.05 M this linear fraction is rather small, it

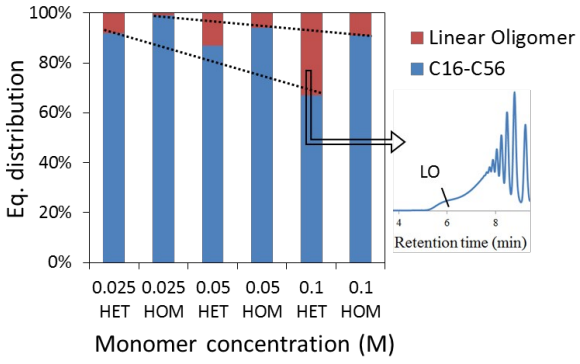

Figure 12. Equilibrium distribution of a homo- and heterogeneous metathesis of *cis*-cyclooctene at different monomer concentrations. Inset: GPC chromatogram of a heterogeneous 0.1 M reaction. LO: linear oligomer; HET: heterogeneous; HOM: homogeneous. Reaction conditions: See Figure 9 and Figure 10.

View Article Online
DOI: 10.1039/C5CY01895H

reaches a value of 20 % after reaction with 0.1 M cyclooctene (GPC, inset Figure 12) with a corresponding C16-C56 selectivity of 70 % (mass balance of 90 %). Similarly to the reaction with 0.05 M, kinetic dissimilarities were observed at low cyclooctene conversions of reactions with 0.025 M and 0.1 M cyclooctene. Results are summarized in Table 5. On one hand the maximal yield of linear polymer increased with concentration, and due to diffusion problems of cyclooctene in the pores the initial selectivity towards C16-C56 cyclic oligomers increased at 0.1 M. This effect was less outspoken at 0.025 M. Product shifts within the C16-C56 fraction on the other hand were likewise observed at 0.025 and 0.1 M; a lower C16:C24 and C24:C32 ratio at a concentration of 0.025 M is apparent, while the contribution of C40 increased at 0.1 M. Kinetic distribution plots (analogue to Figure 11) were set up for these concentrations in Figure S14.

Table 5. Selectivity towards C16-C56 cyclic oligomers at 5 % conversion at different monomer concentrations.

	0.025M	0.05M	0.1M
Homogeneous	55	52	39
Heterogeneous	53	60	45

Reaction conditions: See Figure 9 and Figure 10.

Based on previous results, it can be deduced that the presence of diffusion issues in confined systems may have a significant contribution to the observed product distribution. Either better mass transport in a more open pore architecture, like in TUD-1, or lower Ru loadings should therefore bring the catalytic outcome of the HG2 supported system silica closer to the homogeneous one.

The impact of the Ru loading on the product selectivity was analysed first, since Figure 8 indicated that the catalytic activity per Ru decreases with increasing Ru density on MCM-41. Reactions were therefore performed with 0.3, 0.6 and 1.2 wt% Ru on MCM-41 and their product distributions were compared. At low cyclooctene concentrations, the contribution of linear polymer augments with higher Ru-loaded catalysts (at 20-30 % conversion). As was mentioned above, cyclic oligomers are mainly formed through polymer back-biting in absence of space restriction. But inside the pores of MCM-41, polymer accumulation occurs because the back-biting is slow due to pore restrictions, followed by a slow diffusion of the cyclic oligomers larger than cyclooctene out of the pores, meanwhile also reacting to linear polymers. With increasing Ru loading, the probability of cyclic oligomers to react further into linear polymer is therefore enhanced. As a result, pore obstruction makes the active site less accessible for cyclooctene resulting into lower TOF_i's (*vide supra*, Figure 8). At the end of the reaction significant amounts of carbon residue, expectedly hold inside the catalyst pores, were analysed by TGA. Existence of such carbon residue prevents the reaction of reaching a product distribution according to the thermodynamic equilibrium, and this was indeed manifested in the product distribution. At full conversion, the yield of C16-C56 cyclic oligomers only amounts to 71 % with 0.6 wt% Ru and 42 % with 1.2 wt% Ru; moreover, the perceived distribution within the C16-C56 fraction resembles a kinetic product distribution (Figure S15). Both phenomena confirm a non-equilibrium state after reaction with highly Ru loaded MCM-41.

Next, to further examine the relationship between the product distribution and pore restrictions, two other heterogeneous catalysts with more open pore systems were investigated as well, *i.e.* TUD-1 and KIT-5. Recalling the data of Table 1, HG2/KIT-5 has a cage-like pore system and showed a much lower TOF_i compared to HG2/MCM-41, while HG2/TUD-1 has a three-dimensional pore system with 8-15 nm pores and showed slightly higher TOF_i. The selectivity to C16-C56 cyclic oligomers and linear chains was compared between the three catalysts and presented in Figure 13**.** As shown before, TUD-1 with its open structure and containing 0.21 wt% of Ru, experiences almost no pore diffusion limitation, and indeed the reaction pattern of the cyclic oligomers closely resembles that of the homogeneous reaction (Figure 9A). The formation of the C16-C56 fraction with HG2/KIT-5, in contrast, bear resemblance to the pattern of HG2/MCM-41, but only attains a final C16-C56 selectivity of 75 %. More surprisingly, almost no linear chains are noticed. Obstruction of polymer in the cages is the most obvious explanation impeding the polymer of diffusing out of the silica particle. Only 75 % of the mass was analysed in solution at the end of reaction, while the deficient part was found on the spent catalyst using TGA analysis.

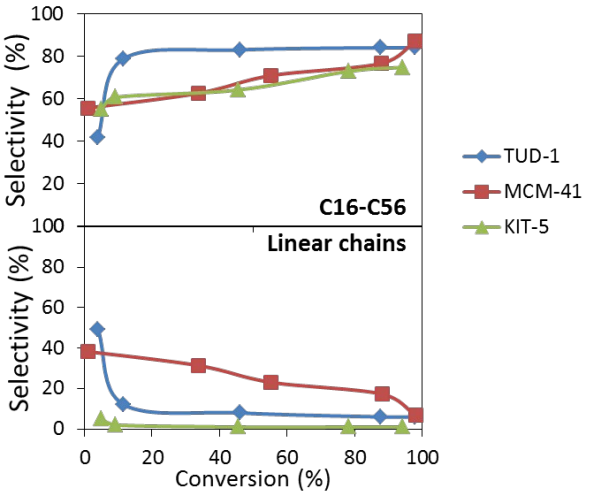

Figure 13. Selectivity towards the C16-C56 fraction (upper figure) and linear chains (lower figure) with HG2/TUD-1 (0.21 wt%), HG2/MCM-41 (0.30 wt%) and HG2/KIT-5 (0.31 wt%). Reaction conditions: See Figure 10.

The main differences between homo- and heterogeneous metathesis of cyclooctene are summarized in the reaction scheme in Figure 14. Linear polymerization dominates the direct formation of cyclic oligomers under homogeneous conditions, causing cyclic oligomers to be formed primarily through back-biting of the linear polymer chains. This effect is most outspoken at high cyclooctene concentration. Heterogeneous reactions with low Ru loadings supported on silica with large pores and an open pore architecture like TUD-1, proceed similarly, and therefore sufficiently high contact times are advised for reactions with these catalysts in continuous fixed-bed plug flow reactors.

Heterogeneous reactions under conditions of pore restriction (or high Ru loading), like in case of HG2/MCM-41, exhibit large differences hereto. They perform under diffusional control leading to slower reaction rates. Because of the diffusional regime, mixtures of linear and cyclic oligomers are formed, which only turn into comparable cyclic oligomers at full conversion. Yet, the reaction proceeds slower (per Ru) and therefore these catalysts are less interesting for production of cyclic rings from cyclooctene.

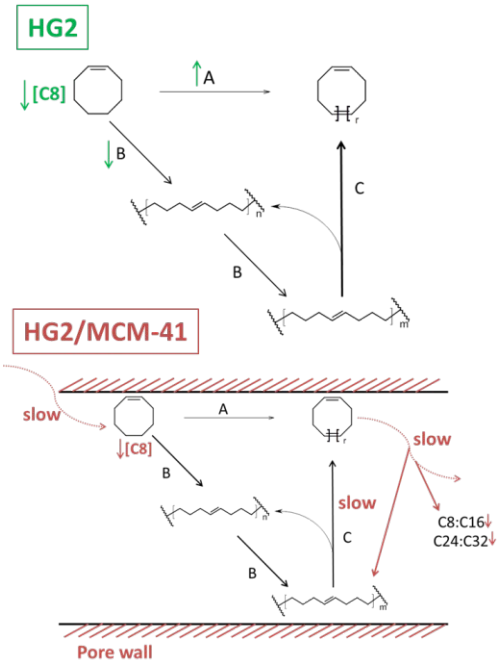

Figure 14. Proposed reaction scheme for the ring-chain distribution of cyclooctene with HG2 (green) and HG2/MCM-41 (red) under steady state circumstances. Route A: direct formation of cyclic oligomers from cyclooctene. Route B: polymerization of cyclooctene to linear chains (n < m). Route C: back-biting of the polymer chain to cyclic oligomers.

Use of HG2/TUD-1 in several metathesis reaction types

Being the best catalyst of choice, HG2/TUD-1 was further exploited in ROMP (Table 6, entry 1-3), ring-closing metathesis (RCM) (Table 6, entry 4-5) and cross-metathesis (CM) reactions (Table 6, entry 6-8) of other substrates. For cyclooctadiene (Table 6, entry 2), the initial TOF was lower than its mono-unsaturated counterpart (Table 6, entry 1), but cyclic oligomers were selectively produced. The ROMP of norbornene (Table 6, entry 3) was conducted at a lower concentration of 0.005 M due to its high reactivity as a consequence of the presence of internal bridges. Full conversion was already reached after 15 minutes. The catalyst also showed good activities in the ring-closing metathesis reactions of diethyl diallyl malonate (Table 6, entry 4) and 1,7-octadiene (Table 6, entry 5), as high TOF_i's were obtained and full conversion was reached after 90 minutes. These two substrates were subjected to additional catalytic tests to evaluate the catalysts robustness in RCM reactions at low catalyst loadings. With 0.5 M of diethyl diallylmalonate and 1,7-octadiene, 0.06 mol % HG2/TUD-1 (0.21 wt% Ru) at 35 °C, TONs of 1290 and 1350 were obtained, respectively. Self-metathesis of methyl oleate (Table 6, entry 6) to 9-octadecene-1,18-dioate, a valuable intermediate for the production of polymers and fine chemicals, was also very successful, even at low catalyst concentration. Cross-metathesis of methyl-10-undecenoate was accomplished at 50 °C, yet 2.5 mol% Ru was needed to reach full conversion (Table 6, entry 7). CM of terminal olefins is known to be more challenging, as it lacks the ring-strain release of ROMP and the entropic driving force of RCM.[111] Finally, the cross-metathesis of butyl vinyl glycolate (Table 6, entry 8) was conducted. This novel renewable substrate can be derived in the methyl ester form from glycolaldehyde and tetroses.[2,59,60] Transesterification with *n*-butanol makes this compound more soluble in hexane. The dimeric product, which is formed in high yields at 50 °C with 1.2 mol% ruthenium, can be a valuable intermediate in the production of new bio-based polymers.[4]

Conclusion

2nd generation Hoveyda-Grubbs (HG2) was immobilized on a series of porous silica materials and tested in the metathesis of *cis*-cyclooctene. High density of silanols are required to firmly anchor HG2, geminal types showing the highest affinity. The affinity of the silica surface for HG2 reduces with HG2 loading. Loadings above 2 wt% should therefore be avoided as they cause HG2 leaching. Cages in the silica pore structure should also be avoided as they root to HG2 degeneration.

The metathesis reaction proceeds under chemical regime, and therefore efficient in HG2, as long as the pore dimensions are large enough, the pore structure sufficiently open and the loading of HG2 not too high. Under such circumstances, cyclooctene is converted to linear polymers, which undergo conversion to the desired cyclic oligomers through back-biting. Reactions rates may be as high as that of the homogeneous reaction and product distributions are identical under conditions of high contact times. If the above criteria are not fulfilled, diffusional control will govern the reaction rate and the product selectivity, leading to slower reaction rates and mixtures of linear polymers and cyclic oligomers. Only under very high contact times, the thermodynamic product distribution, mainly containing cyclic oligomers, is obtained.

Presence of water seems not detrimental to HG2, but its presence in the pores retards the metathesis reaction. Therefore, water removal is advised, prior to HG2 immobilisation. Care has to be taken though to keep the silanol density high to ensure firm anchorage of HG2 and to avoid formation of reactive siloxanes, which chemically react with and destroy HG2.

Overall, TUD-1 with its large pores and open structure, loaded with 0.2 wt% Ru (1.2 wt% HG2), was recognized as the most privileged catalyst to perform ROMP of cyclic olefins. With this immobilized catalyst, a TON of 18.000 was reached in a continuous experiment under non-optimized ambient conditions. This catalyst performed also excellent in other metathesis types. In particular the catalyst appears performant for conversion of biobased substrates like methyl oleate and butyl vinyl glycolate, indicating that immobilized metathesis

View Article Online
DOI: 10.1039/C5CY01897H

Table 6. Various metathesis reactions (ROMP, RCM and CM) performed with HG2/TUD-1.[a]

Entry	Substrate	Product	Time [min] (T [°C])	Conv.[%] [TOF (h^{-1})]	Conv. Split 15 min [%]	Conv. Split End [%]
1		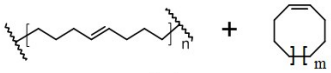	90 (35)	96 [360]	40	40
2			90 (35)	99 [126]	13	12
3[b]		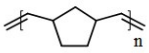	15 (35)	99 [342]	57 [f]	58
4	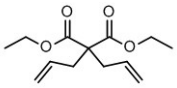	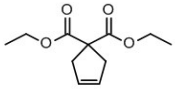	90 (35)	99 [306]	32	33
5	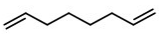		90 (35)	98 [468]	52	52
6[e]	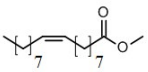	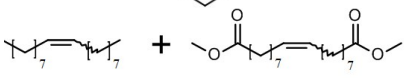	180 (35)	83 [470]	51	51
7[c]	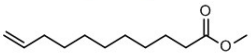	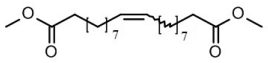	90 (50)	98 [138]	86 [g]	86
8[d,e]	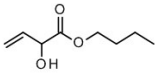	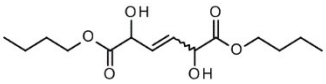	90 (60)	90 [330]	87 [g]	88

[a] 0.05 M substrate; internal standard n-undecane; 5 mL hexane; 0.4 mol % Ru; 35 °C. [b] 0.005 M substrate; [c] 2.5 mol % Ru; [d] 1.2 mol % Ru. [e] Reactions were performed in nonane under reduced pressure (700 mbar) to efficiently remove ethylene. [f] Split test after 5 min. [g] Split test after 10 min.

catalysts can play an important role in the conversion of biomass like oils [112-115] and biomass derived olefins[103, 104,116] to commodity chemicals like polymer building blocks.[4]

Experimental

Synthesis and characterization of the support

The following silica materials were synthesized according to literature: TUD-1,[117] MCM-41,[74] SBA-15 (rope morphology),[118] SBA-15 (fiber morphology),[119] MCM-48,[120] KIT-6,[121] SBA-3,[122] SBA-16,[82] KIT-5,[77] Si-VPI-5,[123] Silicalite-1,[124] and $AlPO_4$-5.[125] Silica Gel 239 (Grace) and Silica Gel 60 (Davisil grade, Sigma-Aldrich) were used as received. Scanning electron microscope (SEM) images were recorded on a JEOL JSM-6010 JV microscope. Before measurements, the materials were coated with gold using a JEOL JSC-1300 sputter. Crystallinity of the mesoporous materials was verified with small angle X-ray scattering (SAXS) on a SMART 6000 diffractometer with Cu source and a 2D CCD detector. Determination of the textural parameters of the support was done by nitrogen physisorption on a Micrometrics TriStar 3000 Surface and Porosity Analyzer. The pore size is calculated according to non-local density functional theory methods[126-128] and pore volumes were determined with the t-plot method. Quantification of the silica silanols was done by FT-IR spectroscopy. Spectra were recorded on a Nicolet 6700 spectrometer, equipped with a DGTS detector and KBr beam splitter (256 scans, resolution of 2 cm^{-1}). Self-supporting wafers were placed in a vacuum IR-cell and dehydrated under vacuum for 1 h at 50 °C prior to measurements. The dry samples were heated progressively at 5 °C min^{-1} and kept at each temperature for 45 minutes. All of the samples (except the one dried at 50 °C) were measured at 150 °C. The molar integrated absorption coefficient $\varepsilon_{(\nu+\delta)}OH$ used was 0.16 cm μmol^{-1}.[84] Near-infrared diffuse reflectance measurements (NIR DRS) were recorded on an Agilent Cary 5000 spectrophotometer. Samples were placed in a quartz tube with window, and were dried at 50 °C under vacuum (10 mbar) or at 150 °C (atmospheric pressure), before measurement. ^{29}Si MAS NMR spectra were recorded on a Bruker AMX300 spectrometer (B_0=7.0 T). At this field, the resonance frequency of ^{29}Si is 59.6 MHz. The samples were packed in a 4 mm Zirconia rotor. Tetramethylsilane was used as chemical shift reference. 2056 scans were accumulated with a recycle delay of 120 s. The spinning frequency of the rotor was 6000 Hz. For determination of the presence of reactive strained siloxanes on MCM-41 and TUD-1, the supports were thermally pretreated under a nitrogen atmosphere at 900 °C and 700 °C, respectively. The dried samples were reacted with dichlorodimethylsilane (DCDMS) under nitrogen atmosphere to cover all surface hydroxyls, followed by drying under vacuum. The silanol-deactivated powders were introduced in a U-tube reactor and brought in contact with a NH_3 flow (3 mL/s) and heated to 500 °C, maintaining this temperature for 6 h to react with strained siloxanes.[129] To verify the covering of surface hydroxyls by DCDMS and siloxane reaction with NH_3, FT-IR spectra were taken as described above. TGA analyses were applied on a TGA Q500 (TA Instruments). Determination of the water amount in the pores was done under a flow of dry nitrogen from room temperature to 500 °C at a heating rate of 3 °C min^{-1}.

Immobilization support and characterization heterogeneous catalyst

Immobilization of the Hoveyda-Grubbs 2nd generation catalyst (HG2) (Sigma-Aldrich, 97 %) was performed in an inert nitrogen atmosphere. The precatalyst was dissolved in toluene (Acros Organics, 99.5 %) and added to the pre-dried silica

source. Typically, a 1.57 mmol L^{-1} solution of HG2 in toluene (5 mL) was added to 0.2 g of a silica support, resulting in a loading of 0.2-0.3 wt% Ru. The suspension is stirred at room temperature for 45 minutes, filtered and washed thoroughly with hexane (Chem-lab, 99 %). After drying, a green powder is obtained, which is stored at -20 °C to guarantee stability. Determination of the amount of Ruthenium immobilized on the support was performed with UV-VIS spectroscopy analysis of the toluene solution before and after immobilization, using a Shimadzu UV-1650PC spectrophotometer. ICP-AES was performed to measure the amount of Ruthenium in solution and to confirm the amount of Ruthenium immobilized on the support. Analyses were conducted on a Jobin Yvon Emmission Ultima ICP with argon plasma. Measurements of the atomic emission spectra of ruthenium were done at 240.727 nm. Before measurements, the samples were dissolved in a light acidic solution (3 % HNO_3 in water). Measurements of the immobilized catalysts after reaction to determine the remaining carbon fraction were performed with TGA under a flow of dry oxygen. The weight loss was monitored from room temperature to 600 °C at a heating rate of 3 °C min^{-1}. Determination of the amount of water in the pores was done under a flow of dry nitrogen from room temperature to 500 °C at a heating rate of 3 °C min^{-1}.

Catalytic reactions

The following substrates were used: *cis*-cyclooctene (Acros Organics, 95 %), *cis*,*cis*-1,5-cyclooctadiene (Sigma Aldrich, ≥99 %), norbornene (Sigma-Aldrich, 99 %), diethyl diallylmalonate (Sigma Aldrich, 98 %), methyl oleate (Sigma-Aldrich, 99 %), methyl 10-undecenoate (Merck, ≥ 96 %), 1,7-octadiene (Alfa Aesar, 97 %) and methyl(D,L)2-hydroxy-3-butenoate (TCI chemicals, > 96 %). For batch reactions, glass reactor vials (10 mL) were charged with the catalyst under an atmosphere of nitrogen (except for a catalyst with a non-thermally pretreated support, e.g. MCM-41 at 25 °C). Stirring tests with increasing amounts of catalysts pointed out that an ideal stirring is only obtained when using 50 mg or less (Figure S16) per 5 mL solvent. With higher amounts, the contact times needed to reach the same conversion increases due to deficient stirring. Therefore standard reactions were performed with 50 mg of catalyst. The substrate was dissolved in hexane (5 mL) and added to the glass reactor. The mixture was stirred at 35 °C, unless mentioned otherwise. n-Undecane (Acros Organics, 99 %) was added as an internal standard whenever required. Ethyl vinyl ether (Sigma Aldrich, 99 %) was used as a terminating agent prior to filtration/centrifugation of the heterogeneous catalyst when taking samples. For cross-metathesis and ring-closing metathesis reactions of terminal olefins an additional balloon filled with argon was used to dilute ethylene formed during reaction when hexane was used as a solvent, while for high-boiling compounds the reaction was performed in hexane under reduced pressure (700 mbar) to remove ethylene. To verify the heterogeneity of the catalyst, a split-test was carried out. After 15 minutes, 2 samples were taken from the reaction mixture. One was quenched with potassium 2-isocyanoacetate (Sigma Aldrich, 85 %) in methanol to quickly deactivate the catalyst, the other sample was filtered with a 0.45 µm PTFE filter to retain the immobilized catalyst and was further stirred at the same reaction temperature. The conversion of the filtered sample was compared to the quenched sample at the end of the reaction. For continuous reactions, a glass reactor was charged with the catalyst (110 mg of HG2/TUD-1, 0.20 wt% Ru; mixed with unloaded pellets of TUD-1) and kept in place by quartz-wool and glass beads. Cyclooctene (0.4 mol L^{-1}) was pumped at a rate of 80 mL h^{-1} over the catalyst bed at room temperature.

Analysis: GC analysis of the volatile products was carried out on an Agilent 6890 GC equipped with a flame-ionization detector (FID) and separated over a HP-5 capillary column. Identification of the reaction products was done with GC-MS on an Agilent 6890N GC with an Agilent 5973N Mass Selective Detector, separated over a HP-5 column. GPC analysis was performed for the separation of bigger oligomers, using a Waters e2695 Separations Module and a Waters 2414 RI detector. The stationary phase consists of a Varian M-Gel 3 mixed column. A 1 mL min^{-1} flow of THF was used. Polystyrene standards were used for calibration. Molecular weight determined fractions: cyclic oligomers, i.e. C16-C56 oligomers of cyclooctene (M_w= 220 – 770 g/mol) or > C56 if mentioned; linear oligomers, i.e. short linear fragments of cyclooctene (M_w= 200 – 3000 g/mol); linear polymer (M_w > 3000 g/mol). ^{1}H-NMR spectra were recorded on a Bruker Avance 300MHz spectrometer using DMSO as a solvent.

Acknowledgements

A.D and B.S thank FWO-Flanders for its financial support (Project G.0229.12).The authors are grateful to Johan Martens for general financial support through Methusalem. Kristof Houthoofd is thanked for NMR measurements and interpretation of the data, Iris Cuppens for ICP-AES, Stef Kerkhofs and Gert Brabants for the SAXS measurements and Walter Vermandel for his help with the continuous experiments. Ivo Stassen is thanked for the NLDFT calculations.

Notes and references

1 1. K. C. Nicolaou, P. G. Bulger and D. Sarlah, *Angew. Chem. Int. Ed.*, 2005, **44**, 4490-4527.

2 2. R. H. Grubbs, *Tetrahedron*, 2004, **60**, 7117-7140.

3 3. R. H. Grubbs and S. Chang, *Tetrahedron*, 1998, **54**, 4413-4450.

4 4. M. Dusselier, P. Van Wouwe, S. De Smet, R. De Clercq, L. Verbelen, P. Van Puyvelde, F. E. Du Prez and B. F. Sels, *ACS Catalysis*, 2013, **3**, 1786-1800.

5 5. C. Samojlowicz, M. Bieniek and K. Grela, *Chem. Rev.*, 2009, **109**, 3708-3742.

6 6. P. Schwab, R. H. Grubbs and J. W. Ziller, *J. Am. Chem. Soc.*, 1996, **118**, 100-110.

7 7. J. C. Mol, *J. Mol. Catal. A: Chem.*, 2004, **213**, 39-45.

8 8. H. Clavier, K. Grela, A. Kirschning, M. Mauduit and S. P. Nolan, *Angew. Chem. Int. Ed.*, 2007, **46**, 6786-6801.

9 9. H. D. Maynard and R. H. Grubbs, *Tetrahedron Lett.*, 1999, **40**, 4137-4140.

10 10. G. C. Vougioukalakis, *Chem. Eur. J.*, 2012, **18**, 8868-8880.

11 11. M. S. Sanford, J. A. Love and R. H. Grubbs, *J. Am. Chem. Soc.*, 2001, **123**, 6543-6554.

12 12. M. Ulman and R. H. Grubbs, *The Journal of Organic Chemistry*, 1999, **64**, 7202-7207.

13 13. J. C. Conrad and D. E. Fogg, *Curr. Org. Chem.*, 2006, **10**, 185-202.

14 14. R. Buffon, A. Choplin, M. Leconte, J. M. Basset, R. Touroude and W. A. Herrmann, *J. Mol. Catal.*, 1992, **72**, L7-L10.

15 15. M. Chabanas, A. Baudouin, C. Copéret and J.-M. Basset, *J. Am. Chem. Soc.*, 2001, **123**, 2062-2063.

16 16. R. P. Saint-Arroman, M. Chabanas, A. Baudouin, C. Copéret, J.-M. Basset, A. Lesage and L. Emsley, *J. Am. Chem. Soc.*, 2001, **123**, 3820-3821.

17 17. M. P. Conley, W. P. Forrest, V. Mougel, C. Copéret and R. R. Schrock, *Angew. Chem.*, 2014, **126**, 14445-14448.

18 18. V. Mougel, C. B. Santiago, P. A. Zhizhko, E. N. Bess, J. Varga, G. Frater, M. S. Sigman and C. Copéret, *J. Am. Chem. Soc.*, 2015, **137**, 6699-6704.

19 19. T. S. Halbach, S. Mix, D. Fischer, S. Maechling, J. O. Krause, C. Sievers, S. Blechert, O. Nuyken and M. R. Buchmeiser, *J. Org. Chem.*, 2004, **70**, 4687-4694.

20 20. J. O. Krause, S. H. Lubbad, O. Nuyken and M. R. Buchmeiser, *Macromol. Rapid Commun.*, 2003, **24**, 875-878.

21 21. J. O. Krause, O. Nuyken, K. Wurst and M. R. Buchmeiser, *Chem. Eur. J.*, 2004, **10**, 777-784.

22 22. D. Bek, N. Žilková, J. Dědeček, J. Sedláček and H. Balcar, *Top. Catal.*, 2009, **53**, 200-209.

23 23. P. Nieczypor, W. Buchowicz, W. J. N. Meester, F. P. J. T. Rutjes and J. C. Mol, *Tetrahedron Lett.*, 2001, **42**, 7103-7105.

24 24. K. Vehlow, S. Maechling, K. Köhler and S. Blechert, *J. Organomet. Chem.*, 2006, **691**, 5267-5277.

25 25. L. Yang, M. Mayr, K. Wurst and M. R. Buchmeiser, *Chem. Eur. J.*, 2004, **10**, 5761-5770.

26 26. D. Bek, H. Balcar, N. Žilková, A. t. Zukal, M. Horáček and J. i. Čejka, *ACS Catalysis*, 2011, **1**, 709-718.

27 27. L. Li and J.-l. Shi, *Adv. Synth. Catal.*, 2005, **347**, 1745-1749.

28 28. S. Randl, N. Buschmann, S. J. Connon and S. Blechert, *Synlett*, 2001, **10**, 1547-1550.

29 29. M. Mayr, B. Mayr and M. R. Buchmeiser, *Angew Chem Int Ed*, 2001, **40**, 3839-3842.

30 30. J. P. Gallivan, J. P. Jordan and R. H. Grubbs, *Tetrahedron Lett.*, 2005, **46**, 2577-2580.

31 31. K. Melis, D. E. De Vos, P. A. Jacobs and F. Verpoort, *J. Mol. Catal. A: Chem.*, 2001, **169**, 47-56.

32 32. K. H. Park, S. Kim and Y. K. Chung, *Bull. Korean Chem. Soc.*, 2008, **29**, 2057-2060.

33 33. A. Monge-Marcet, R. Pleixats, X. Cattoën and M. Wong Chi Man, *J. Mol. Catal. A: Chem.*, 2012, **357**, 59-66.

34 34. S. T. Nguyen and R. H. Grubbs, *J. Organomet. Chem.*, 1995, **497**, 195-200.

35 35. S. C. Schürer, S. Gessler, N. Buschmann and S. Blechert, *Angew Chem Int Ed*, 2000, **39**, 3898-3901.

36 36. I. Karamé, M. Boualleg, J.-M. Camus, T. K. Maishal, J. Alauzun, J.-M. Basset, C. Copéret, R. J. P. Corriu, E. Jeanneau, A. Mehdi, C. Reyé, L. Veyre and C. Thieuleux, *Chem. Eur. J.*, 2009, **15**, 11820-11823.

37 37. A. G. M. Barrett and S. M. R. Cramp, Richard S., *Org. Lett.*, 1999, **1**, 1083-1086.

38 38. G. Borja, R. Pleixats, R. Alibés, X. Cattoën and M. W. C. Man, *Molecules*, 2010, **15**, 5756-5767.

39 39. X. Elias, R. Pleixats, M. W. C. Man and J. J. E. Moreau, *Adv. Synth. Catal.*, 2007, **349**, 1701-1713.

40 40. D. Fischer and S. Blechert, *Adv. Synth. Catal.*, 2005, **347**, 1329-1332.

41 41. S. B. Garber, J. S. Kingsbury, B. L. Gray and A. H. Hoveyda, *J. Am. Chem. Soc.*, 2000, **122**, 8168-8179.

42 42. A. Keraani, C. Fischmeister, T. Renouard, M. Le Floch, A. Baudry, C. Bruneau and M. Rabiller-Baudry, *J. Mol. Catal. A: Chem.*, 2012, **357**, 73-80.

43 43. J. S. Kingsbury, S. B. Garber, J. M. Giftos, B. L. Gray, M. M. Okamoto, R. A. Farrer, J. T. Fourkas and A. H. Hoveyda, *Angew Chem Int Ed*, 2001, **40**, 4251-4256.

44 44. J. Lim, S. S. Lee, S. N. Riduan and J. Y. Ying, *Adv. Synth. Catal.*, 2007, **349**, 1066-1076.

45 45. J. Lim, S. Seong Lee and J. Y. Ying, *Chem. Commun.*, 2010, **46**, 806.

46 46. S. Varray, R. Lazaro, J. Martinez and F. Lamaty, *Organometallics*, 2003, **22**, 2426-2435.

47 47. Q. Yao, *Angew Chem Int Ed*, 2000, **39**, 3896-3898.

48 48. H. Zhang, Y. Li, S. Shao, H. Wu and P. Wu, *J. Mol. Catal. A: Chem.*, 2013, **372**, 35-43.

49 49. Q. T. Easter, V. Trauschke and S. A. Blum, *ACS Catalysis*, 2015, **5**, 2290-2295.

50 50. H. Staub, F. Kleitz and F.-G. Fontaine, *Microporous Mesoporous Mater.*, 2013, **175**, 170-177.

51 51. H. Yang, Z. Ma, T. Zhou, W. Zhang, J. Chao and Y. Qin, *ChemCatChem*, 2013, **5**, 2278-2287.

52 52. Q. Li, T. Zhou and H. Yang, *ACS Catalysis*, 2015, **5**, 2225-2231.

53 53. C. Copéret and J. M. Basset, *Adv. Synth. Catal.*, 2007, **349**, 78-92.

54 54. H. Balcar and J. Čejka, *Coord. Chem. Rev.*, 2013, **257**, 3107-3124.

55 55. H. Balcar and J. Čejka, *Macromolecular Symposia*, 2010, **293**, 43-47.

56 56. M. P. Conley, C. Copéret and C. Thieuleux, *ACS Catalysis*, 2014, **4**, 1458-1469.

57 57. F. B. Hamad, C. Kai, Y. Cai, Y. Xie, Y. Lu, F. Ding, Y. Sun and F. Verpoort, *Curr. Org. Chem.*, 2013, **17**, 2592-2608.

58 58. B. Van Berlo, K. Houthoofd, B. F. Sels and P. A. Jacobs, *Adv. Synth. Catal.*, 2008, **350**, 1949-1953.

59 59. J. Cabrera, R. Padilla, M. Bru, R. Lindner, T. Kageyama, K. Wilckens, S. L. Balof, H.-J. Schanz, R. Dehn, J. H. Teles, S. Deuerlein, K. Müller, F. Rominger and M. Limbach, *Chem. Eur. J.*, 2012, **18**, 14717-14724.

60 60. M. Bru, R. Dehn, J. H. Teles, S. Deuerlein, M. Danz, I. B. Müller and M. Limbach, *Chem. Eur. J.*, 2013, **19**, 11661-11671.

61 61. W. Solodenko, A. Doppiu, R. Frankfurter, C. Vogt and A. Kirschning, *Aust. J. Chem.*, 2013, **66**, 183.

62 62. H. Balcar, T. Shinde, N. Žilková and Z. Bastl, *Beilstein J. Org. Chem.*, 2011, **7**, 22-28.

63 63. H. Yang, Z. Ma, Y. Wang, Y. Wang and L. Fang, *Chem. Commun.*, 2010, **46**, 8659.

64 64. T. Shinde, N. Žilková, V. Hanková and H. Balcar, *Catal. Today*, 2012, **179**, 123-129.

65 65. J. Pastva, K. Skowerski, S. J. Czarnocki, N. Žilková, J. Čejka, Z. Bastl and H. Balcar, *ACS Catalysis*, 2014, **4**, 3227-3236.

66 66. *United States Pat.,* US20120165588, 2012.

67 67. Z. Jia and M. J. Monteiro, *J. Polym. Sci., Part A: Polym. Chem.*, 2012, **50**, 2085-2097.

68 68. H. R. Kricheldorf, *J. Polym. Sci., Part A: Polym. Chem.*, 2010, **48**, 251-284.

69 69. *United States Pat.,* US2553651, 1951.

70 70. *United States Pat.,* US3465016, 1969.

71 71. C. Sell, in *The Chemistry of Fragrances: From Perfumer to Consumer*, ed. C. S. Sell, The Royal Society of Chemistry, Cambridge, 2006, ch. Ingredients for the modern perfumery industry, pp. 95-106.

72 72. M. K. Samantaray, J. Alauzun, D. Gajan, S. Kavitake, A. Mehdi, L. Veyre, M. Lelli, A. Lesage, L. Emsley, C. Copéret and C. Thieuleux, *J. Am. Chem. Soc.*, 2013, **135**, 3193-3199.

73 73. Information about impurities silica gels: Catalog Resins & Media p.5, Sigma-Aldrich.

74 74. B. Pauwels, G. Van Tendeloo, C. Thoelen, W. Van Rhijn and P. Jacobs, *Adv. Mater.*, 2001, **13**, 1317-1320.

75 75. H. Zhang, J. Sun, D. Ma, X. Bao, A. Klein-Hoffmann, G. Weinberg, D. Su and R. Schlögl, *J. Am. Chem. Soc.*, 2004, **126**, 7440-7441.

76 76. S. Polarz, B. Völker and F. Jeremias, *Dalton Transactions*, 2010, **39**, 577-584.

77 77. F. Kleitz, D. Liu, G. M. Anilkumar, I.-S. Park, L. A. Solovyov, A. Shmakov, N. and R. Ryoo, *The Journal of Physical Chemistry B*, 2003, **107**, 14296-14300.

78 78. H.-J. Kim, K.-S. Jang, P. Galebach, C. Gilbert, G. Tompsett, W. C. Conner, C. W. Jones and S. Nair, *Journal of Membrane Science*, 2013, **427**, 293-302.

79 79. Z. Shan, J. C. Jansen, L. Marchese and T. Maschmeyer, *Microporous Mesoporous Mater.*, 2001, **48**, 181-187.

80 80. S. Telalovic, A. Ramanathan, G. Mul and U. Hanefeld, *J. Mater. Chem.*, 2010, **20**, 642-658.

81 81. R. Maheswari, R. Anand and G. Imran, *J. Porous Mater.*, 2012, **19**, 283-288.

82 82. F. Kleitz, T.-W. Kim and R. Ryoo, *Langmuir*, 2006, **22**, 440-445.

83 83. L. T. Zhuravlev, *Colloids Surf., A*, 2000, **173**, 1-38.

84 84. J.-P. Gallas, J.-M. Goupil, A. Vimont, J.-C. Lavalley, B. Gil, J.-P. Gilson and O. Miserque, *Langmuir*, 2009, **25**, 5825-5834.

85 85. A. A. Christy, *Advanced Materials Research*, 2013, **650**, 66-71.

86 86. K. Wan, Q. Liu and C. Zhang, *Mater. Lett.*, 2003, **57**, 3839-3842.

87 87. S. Shioji, M. Hanada, Y. Hayashi, K. Tokami and H. Yamamoto, *Adv. Powder Technol.*, 2007, **18**, 467-483.

88 88. P. Der Voort, *J. Chem. Soc., Faraday Trans.*, 1990, **86**, 3747-3750.

89 89. K. Unger, *Porous Silica*, Elsevier Science, 1979.

90 90. D. W. Sindorf and G. E. Maciel, *J. Am. Chem. Soc.*, 1983, **105**, 3767-3776.

91 91. B. Fubini, V. Bolis, A. Cavenago and P. Ugliengo, *J. Chem. Soc., Faraday Trans.*, 1992, **88**, 277-289.

92 92. J. P. Blitz, C. C. Meverden and R. E. Diebel, *Langmuir*, 1998, **14**, 1122-1129.

93 93. B. A. Morrow, I. A. Cody and L. S. M. Lee, *J. Phys. Chem.*, 1976, **80**, 2761-2767.

94 94. H. Staub, R. Guillet-Nicolas, N. Even, L. Kayser, F. Kleitz and F.-G. Fontaine, *Chem. Eur. J.*, 2011, **17**, 4254-4265.

95 95. M. Ide, M. El-Roz, E. De Canck, A. Vicente, T. Planckaert, T. Bogaerts, I. Van Driessche, F. Lynen, V. Van Speybroeck, F. Thybault-Starzyk and P. Van Der Voort, *PCCP*, 2013, **15**, 642.

96 96. J. D. Robert, in *Catalysis for the Conversion of Biomass and Its Derivatives*, eds. M. Behrens and A. K. Datye, The Max Planck Research Library for the History and Development of Knowledge, Berlin, 2013, pp. 255-286.

97 97. D. Luss, *Diffusion-Reaction Interactions in Catalyst Pellets*, Taylor & Francis, Texas, 1986.

98 98. S. Monfette and D. E. Fogg, *Chem. Rev.*, 2009, **109**, 3783-3816.

99 99. H. Höcker, W. Reimann, L. Reif and K. Riebel, *J. Mol. Catal.*, 1980, **8**, 191-202.

100 100. L. Reif and H. Hoecker, *Macromolecules*, 1984, **17**, 952-956.

101 101. H. Jacobson and W. H. Stockmayer, *The Journal of Chemical Physics*, 1950, **18**, 1600-1606.

102 102. Z. R. Chen, J. P. Claverie, R. H. Grubbs and J. A. Kornfield, *Macromolecules*, 1995, **28**, 2147-2154.

103 103. A. Blencowe and G. G. Qiao, *J. Am. Chem. Soc.*, 2013, **135**, 5717-5725.

104 104. S. Kavitake, M. K. Samantaray, R. Dehn, S. Deuerlein, M. Limbach, J. A. Schachner, E. Jeanneau, C. Copéret and C. Thieuleux, *Dalton Transactions*, 2011, **40**, 12443.

105 105. S. M. Rountree, M. C. Lagunas, C. Hardacre and P. N. Davey, *Applied Catalysis A: General*, 2011, **408**, 54-62.

View Article Online
DOI: 10.1039/C5CY01897H

106 106. B. Van Berlo, J. Dijkmans, K. Houthoofd, M. Tromp, I. Hermans, P. Jacobs and B. F. Sels, Detroit, U.S.A., 2011.
107 107. R. Klaewkla, M. Arend and W. F. Hoelderich, in *Mass Transfer - Advanced Aspects*, ed. H. Nakajima, 2011.
108 108. H. Höcker, W. Reimann, K. Riebel and Z. Szentivanyi, *Die Makromolekulare Chemie*, 1976, **177**, 1707-1715.
109 109. E. Thorn-Csányi and K. Ruhland, *Macromol. Chem. Phys.*, 1999, **200**, 1662-1671.
110 110. C. W. Bielawski and R. H. Grubbs, *Prog. Polym. Sci.*, 2007, **32**, 1-29.
111 111. A. K. Chatterjee, T.-L. Choi, D. P. Sanders and R. H. Grubbs, *J. Am. Chem. Soc.*, 2003, **125**, 11360-11370.
112 112. A. Nickel, T. Ung, G. Mkrtumyan, J. Uy, C. Lee, D. Stoianova, J. Papazian, W.-H. Wei, A. Mallari, Y. Schrodi and R. Pederson, *Top. Catal.*, 2012, **55**, 518-523.
113 113. J. C. Mol and R. Buffon, *Journal of the Brazilian Chemical Society*, 1998, **9**, 1-11.
114 114. J. C. Mol, *Green Chemistry*, 2002, **4**, 5-13.
115 115. R. Kadyrov, C. Azap, S. Weidlich and D. Wolf, *Top. Catal.*, 2012, **55**, 538-542.
116 116. Y. Yang, X. Wei, F. Zeng and L. Deng, *Green Chemistry*, 2015.
117 117. J. C. Jansen, Z. Shan, T. Maschmeyer, L. Marchese, W. Zhou and N. v. d. Puil, *Chem. Commun.*, 2001, 713-714.
118 118. K. Flodström and V. Alfredsson, *Microporous Mesoporous Mater.*, 2003, **59**, 167-176.
119 119. D. Zhao, *Science*, 1998, **279**, 548-552.
120 120. K. Schumacher, M. Grün and K. K. Unger, *Microporous Mesoporous Mater.*, 1999, **27**, 201-206.
121 121. A. Vinu, N. Gokulakrishnan, V. V. Balasubramanian, S. Alam, M. P. Kapoor, K. Ariga and T. Mori, *Chem. Eur. J.*, 2008, **14**, 11529-11538.
122 122. O. A. Anunziata, A. R. Beltramone, M. L. Martínez and L. L. Belon, *J. Colloid Interface Sci.*, 2007, **315**, 184-190.
123 123. S. del Val, T. Blasco, E. Sastre and J. Perez-Pariente, *J. Chem. Soc., Chem. Commun.*, 1995, 731-732.
124 124. C. Shao, X. Li, S. Qiu, F.-s. Xiao and O. Terasaki, *Microporous Mesoporous Mater.*, 2000, **39**, 117-123.
125 125. M. Fang, H. Du, W. Xu, X. Meng and W. Pang, *Microporous Mater.*, 1997, **9**, 59-61.
126 126. P. I. Ravikovitch, G. L. Haller and A. V. Neimark, *Adv. Colloid Interface Sci.*, 1998, **76–77**, 203-226.
127 127. M. Jaroniec, M. Kruk, J. P. Olivier and S. Koch, in *Stud. Surf. Sci. Catal.*, eds. G. K. K.K. Unger and J. P. Baselt, Elsevier, 2000, vol. Volume 128, pp. 71-80.
128 128. J. Landers, G. Y. Gor and A. V. Neimark, *Colloids Surf., A*, 2013, **437**, 3-32.
129 129. T. Asefa, M. Kruk, N. Coombs, H. Grondey, M. J. MacLachlan, M. Jaroniec and G. A. Ozin, *J. Am. Chem. Soc.*, 2003, **125**, 11662-11673.
130
131

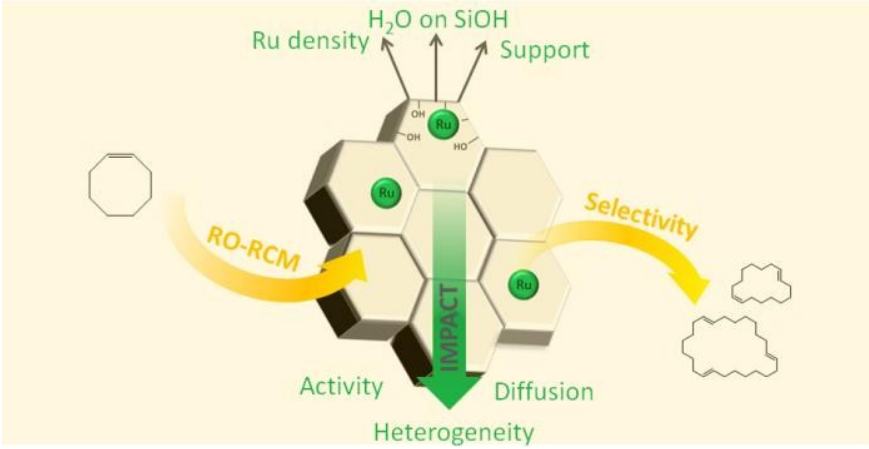

The ideal support characteristics for immobilization of the Hoveyda-Grubbs 2 catalyst were defined in the metathesis of cyclooctene and the reaction mechanism to cyclic oligomers was unraveled.